Title

Heterologous Expression of Nitrogenase Iron Proteins and Investigation of its Extensive Potential

Permalink

https://escholarship.org/uc/item/70n2m6cb

Author

Fathi Rasekh, Mahtab

Publication Date

2022

UNIVERSITY OF CALIFORNIA,
IRVINE

Heterologous Expression of Nitrogenase Iron Proteins and Investigation of its Extensive

Potential

DISSERTATION

submitted in partial satisfaction of the requirements
for the degree of

DOCTOR OF PHILOSOPHY

in Chemistry

by

Mahtab Fathi Rasekh

Dissertation Committee:
Professor Markus W. Ribbe, Chair
Professor Douglas J. Tobias
Professor Celia W. Goulding

2022

DEDICATION

To

my parents and friends

TABLE OF CONTENTS

LIST OF FIGURES

LIST OF TABLES

LIST OF ABBREVIATIONS

[Fe$_4$S$_4$]	Four iron four sulfur
A. vinelandii (Av)	*Azotobacter vinelandii*
ADP	Adenosine diphosphate
Ar	Argon
ATP	Adenosine triphosphate
C. phaeobacteroides (Cp)	*Chlorobium phaeobacteroides*
C$_2$H$_2$	Acetylene
C$_2$H$_4$	Ethylene
C$_2$H$_6$	Ethane
C$_3$H$_6$	Propene
C$_3$H$_8$	Propane
C$_4$H$_{10}$	Butane
C$_4$H$_8$	Butene
CH$_4$	Methane
CO	Carbon monoxide
CO$_2$	Carbon dioxide
CV	Cyclic voltammetry
D. vulgaris (Dv)	*Desulfovibrio vulgaris*
DMF	Dimethylformamide
DT	Dithionite (sodium dithionite)
e$^-$	Electron
E. coli	*Escherichia coli*
E$^{0'}$	Standard reduction potential
EI	Electron impact
E$_m$	Midpoint reduction potential
EPR	Electron paramagnetic resonance
ET	Electron transfer
Eu^{II}- DOTA	Europium (II) 1,4,7,10-tetraazacyclododecane-1,4,7,10-tetraacetic acid
Eu^{II}- DOTAM	Europium (II) 1,4,7,10-tetrakis(carbamoylmethyl)-1,4,7,10-tetraazacyclododecane
Eu^{II} -DTPA	Europium (II) diethylenetriaminepentaacetic acid
Fe-only nitrogenase	Iron-only nitrogenase
FeS	Iron sulfur
FID	Flame ionization detector
FT	Fischer-Tropsch
G	Gauss
G. uraniireducens (Gu)	*Geobacter uraniireducens*
GC	Gas chromatography
GC-MS	Gas chromatography mass spectrometry
H$^+$	Proton
HC	Hydrocarbons
hr	Hour
ICP-OES	Inductively coupled plasma optical emission spectroscopy

IDS	Indigo disulfonite
IMAC	Immobilized metal affinity chromatography
KCl	Potassium chloride
kDa	kiloDalton
L	Liter
LN_2	Liquid nitrogen
M	Molar
M-cluster	Iron molybdenum cofactor
M. acetivorans (Ma)	*Methanosarcina acetivorans*
M. maripaludis (Mmp)	*Methanococcus maripaludis*
M. palustris (Mp)	*Methanosphaerula palustris*
MgADP	Magnesium adenosine diphosphate
MgATP	Magnesium adenosine triphosphate
min	Minute
Mo-nitrogenase	Molybdenum nitrogenase
NMF	N-methylformamide
PDB	Protein data bank
P_i	Inorganic phosphate
P^P-cluster	P-cluster precursor
PMSF	Phenylmethylsulfonyl fluoride
rpm	Rotations per minute
SCE	Saturated calomel electrode
SDS-PAGE	Sodium dodecyl sulfate polyacrylamide gel electrophoresis
SHE	Standard hydrogen electrode
TCD	Thermal conductivity detector
TON	Turnover number
Tris	Tris-(hydroxymethyl)-amino methane
UV-Vis	Ultraviolet-visible
V	Volt
V-nitrogenase	Vanadium nitrogenase
v/v	Volume/volume
w/v	Weight/volume
SAXS	Small-angle X-ray scattering

ACKNOWLEDGEMENTS

First, I would like to thank Dr. Markus Ribbe and Dr. Yilin Hu for all their support, guidance, and the opportunity that they have provided for me.

I would also like to thank to all the students and staff members of both Hu and Ribbe groups that I have had the chance to work with and learn from: Dr. Chi Chung (CC) Lee, Dr. Andrew Jasniewski, Prof. Kazuki Tanifuji, Dr. Martin Steibritz, Dr. Caleb Hiller, Dr. Lee Rettberg, Dr. Wonchull Kang, Dr. Megan Newcomb, Dr. Jasper Liedtke, and Joseph Solomon. I especially want to thank Andrew, Kazuki, and CC for helping me getting through advancement exam.

I am very grateful to Dr. Celia Goulding and Dr. Douglas Tobias for their support and accepting my invitation to be on my dissertation committee.

Finally, I want to express my deepest appreciation to my family, true friends, and Dr. Amir Jadidian. I would not be able to do this without their indefinite and selfless support, encouragement, and love.

VITA

Mahtab Fathi Rasekh

Education

University of California Irvine, CA	**2017-2022**

Ph.D. in Chemistry | GPA: 3.95
Advisor: Prof. Yilin Hu, Prof. Markus W. Ribbe

University of Minnesota Duluth, MN	**2013-2016**

M.Sc. in Chemistry | GPA: 3.53
Advisor: Prof. Victor Nemykin

Sharif University of Technology, Tehran, Iran	**2007-2012**

B. Sc. In Chemistry

Work Experience

University of California Irvine, CA	**2017-2022**

Graduate Research Assistant
- Developed methods for heterologous expression of nitrogenase enzyme homologs in *E. Coli*
- Analyzed and characterized nitrogenase enzyme using SDS-PAGE, GC, HPLC, EPR, UV-Vis, and ICP-EOS.

Graduate Teaching Assistant
- Responsible for preparing lab set up and maintaining the equipment.
- Provided instruction (pre-lab lecture), supervision, and assistance to the students.
- Courses: Organic Chemistry I, II, and III Labs, Microbiology Lab, Chemical Biology Lab, and Lecture.

University of Minnesota Duluth, MN	**2013 –2016**

Graduate Research Assistant
- Developed synthesis and characterization protocols for metal-containing porphyrins.
- Performed analysis on synthesized porphyrins using NMR, IR, UV-Vis, MCD, CV, DPV, and X-Ray crystallography.

Graduate Teaching Assistant
- Responsible for preparing lesson plan, lab set up and maintenance.
- Provided instruction (pre-lab lecture), supervision, and assistance to the students.
- Courses: General Chemistry I and II, Organic Chemistry II, and Aspects of Chemistry Labs and Lecture.

Publications

1. M. Fathi-Rasekh.; Theoretical Study of Borazine: Cation-π (Be^{2+}, Mg $^{2+}$ and Ca^{2+}) Interaction, *Structural Chemistry*, **2012**, 1-7.

2. M. Fathi-Rasekh.; Theoretical Investigation on the Structure and Properties of Alumazine…MComplexes (M = Li^+, Na^+, K^+, Be^{2+}, Mg^{2+} and Ca^{2+}), *Journal of Theoretical and Computational Chemistry*, **2013**, 10, 13500331-135003311.

3. V. N. Nemykin, S. V. Dudkin, M. Fathi-Rasekh, A. D. Spaeth, H. M. Rhoda, R. V. Belosludov, M. V. Barybin.; Probing electronic communications in heterotrinuclear Fe-Ru-Fe molecular wires formed by Ruthenium (II) tetraphenylporphyrin and isocyanoferrocene or 1,1'-diisocyanoferrocene ligands, *Inorganic Chemistry*, **2015**, 54, 10711-10724.

4. P. V. Solntsev, D. R. Anderson, H. M. Rhoda, R. V. Belosludov, M. Fathi-Rasekh, E. Maligaspe, N. N. Gerasimchuk, V. N. Nemykin.; Initial report on molecular and electronic structure of spherical multiferrocenyl / tin(IV) (hydr)oxide $[(FcSn)_{12}O_{14}(OH)_6]X_2$ clusters, *Crystal Growth & Design*, **2016**, 16, 1027-1037.

5. Cidlina, M. Miletin, M. Fathi-Rasekh, V. N. Nemykin, P. Zimcik, V. Novakova.; OFF-ON-OFF red-emitting fluorescence indicators for a narrow pH window, *Chemistry A European Journal*, **2016**, 23, 1795-1804. ***Featured article on the journal cover.***

6. M. Fathi-Rasekh, G. T. Rohde, M. D. Hart, T. Nakakita, R. R. Valiev, M. V. Barybin, V. N. Nemykin.; Positional isomers of isocyanoazulene as axial ligands coordinated to Ruthenium (II) tetraphenylporphyrin: fine tuning of redox and optical properties, *Inorganic Chemistry*, **2019**, 58, 9316-9325.

7. R. K. Swedin, Y. V. Zatsikha, A. T. Healy, N. O. Didukh, T. S. Blesener, M. Fathi-Rasekh, T. Wang, A. J. King, V. N. Nemykin, D. A. Blank.; Rapid excited state deactivation of BODIPY derivatives by a Boron bound Catechol, *Journal of Physical Chemistry Letters*, **2019**, 10, 1828-1832.

8. J. B. Solomon, M. F. Rasekh, C. J. Hiller, C. C. Lee, K. Tanifuji, M. W. Ribbe, Y. Hu.; Probing all-ferrous state of methanogen nitrogenase iron proteins, *JACS Au*, **2020**, 1, 119-123.

9. J. B. Solomon, C. C. Lee, A. J. Jasniewski, M. Fathi-Rasekh, M. W. Ribbe, Y. Hu.; Heterologous expression and engineering of the nitrogenase cofactor biosynthesis scaffold NifEN, *Angewandte Chemie,* **2020**, 132, 6954-6960

ABSTRACT OF THE DISSERTATION

Heterologous Expression of Nitrogenase Iron Proteins and Investigation of its Extensive

Potential

by

Mahtab Fathi Rasekh

Doctor of Philosophy in Chemistry

University of California, Irvine, 2022

Professor Markus W. Ribbe, Chair

Nitrogenase is a key enzyme in the nitrogen cycle, and it is often produced by soil bacteria such as *Azotobacter vinelandii*, green sulfur bacteria, and cyanobacteria. Nitrogenase is a complex metalloenzyme responsible for converting nitrogen gas (N_2) to bioavailable ammonia (NH_3) under ambient conditions to ammonia, a transformation traditionally facilitated by industrial Haber-Bosch process under high temperature and pressure ($\approx$450 °C, >200 atm). The iron protein of nitrogenase is one of two components and plays a key role as a reductase component to transfer electrons to the catalytic component of enzyme. Moreover, it has been discovered that iron protein can reduce carbon monoxide and carbon dioxide to short-chain hydrocarbons (alkanes and alkenes).

There are two major research directions in the study of the nitrogenase system 1) understanding the structure and function of the enzyme as well as its complex metallocofactors to better understand N_2 reduction and hydrocarbon formation and 2) the

heterologous expression of the nitrogenase operon into different microorganisms for the development of microbe-based bioreactors and other biotechnology applications. This work focuses on the generation of a library of iron protein homologs that can be used as a toolbox for mechanistic investigations and to facilitate the heterologous expression of functional nitrogenase based systems. Moreover, this work explores the long-lasting debate of whether the Fe protein can utilize the $[Fe_4S_4]^{0/2+}$ redox couple to support a two-electron transfer during substrate turnover which, therefore, is crucial for expanding our knowledge of the reaction mechanism of nitrogenase and the cellular energetics of nitrogenase-based processes.

CHAPTER 1

Introduction to Nitrogenase

1.1 Overview of Nitrogenase

Nitrogenase is one of the most complex metalloenzymes found in the nature which plays an essential role in the nitrogen cycle. Although there are substantial sources of dinitrogen in the atmosphere, (~78% of earth's atmosphere), dinitrogen (N_2) is not the bioavailable source for plants and microorganisms that can be incorporated into fundamental building blocks of life such as amino acids, proteins, deoxyribonucleic acid (DNA), and ribonucleic acid (RNA). Breaking the triple bond of dinitrogen requires substantial amount of energy (N_2 bond dissociation energy is (~946 kJ/mol). Hence, dinitrogen is not kinetically reactive towards oxidation or reduction. The entire production of ammonia to be used as fertilizer and bioavailable nitrogen source is through an industrial method, known as Haber-Bosch. During the Haber-Bosch process nitrogen and hydrogen gas react under extremely high pressure (~200 atm) and temperature (400-500 °C) to generate ammonia shown in Equation 1.

$$N_{2\,(g)} + 3H_{2\,(g)} \xrightarrow[\text{400-500 °C}]{\text{~200 atm}} 2NH_3 \qquad (1)$$
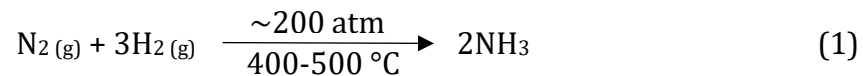
The industrial production of ammonia, not only requires tremendous amounts of energy, usually provided by burning fossil fuels, but also creates significant amounts of greenhouse gases and pollutants.

Fortunately, a group of prokaryotic microorganisms have been discovered with the ability to reduce dinitrogen (N_2) to ammonia (NH_3) under ambient temperature and pressure through a process called nitrogen fixation shown in Equation 2. [1]

$$N_2 + 8H^+ + 16MgATP + 8e^- \longrightarrow 2NH_3 + H_2 + 16MgADP + 16Pi \qquad (2)$$

During past decades nitrogenase containing prokaryotic organisms, specially diazotrophs, have been extensively studied to shed light on nitrogenase enzyme system. [2,3] *Azotobacter vinelandii (Av)* has been found to be the best organism to study nitrogenase due to its amenability to genetic manipulation, nutritional flexibility, ability to fix nitrogen during aerobic growth, and fully sequenced genome. [4-8] So far, three highly related nitrogenase systems have been discovered, which are differentiated by the presence of Molybdenum (Mo), Vanadium (V), or Iron (Fe) in their metallocofactor. [9] Molybdenum nitrogenase requires 11 nitrogen fixation (*nif*) genes to have a fully functioning nitrogen fixation system, including *nif*H, *nif*D, *nif*K, *nif*B, *nif*E, *nif*N, *nif*S, *nif*U, *nif*V, *nif*M, and *nif*Q. [8] Figure 1.1 represents the organization and proposed function of Mo nitrogenase genes in *A. vinelandii*. [10,11]
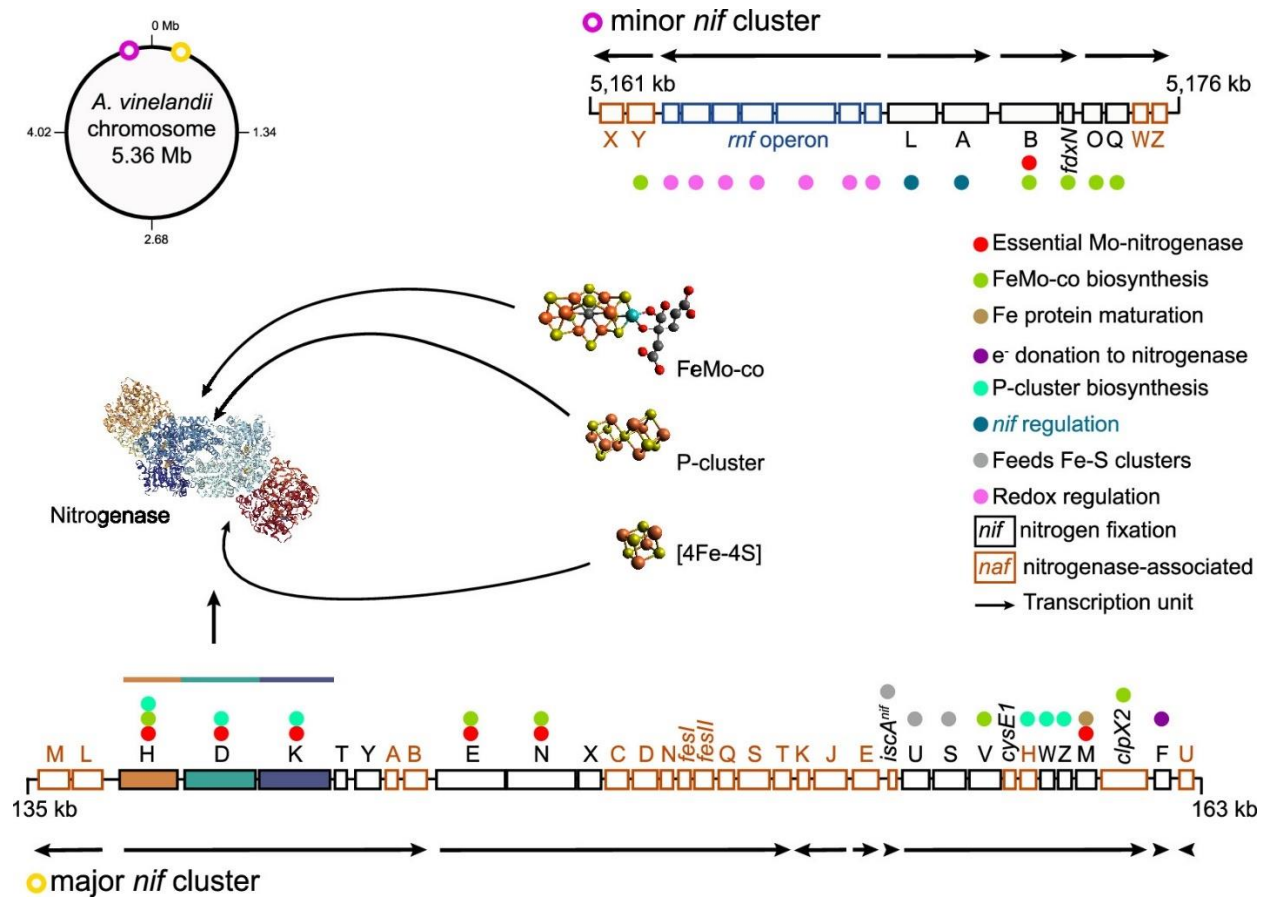
Figure 1.1 Organization and proposed functions of Mo nitrogenase genes in *A. vinelandii*. Chromosomal location and genetic organization of the major and minor *nif* gene clusters are depicted. Numbers to the left and right of each gene cluster indicate chromosomal location. [10]

Furthermore, nitrogenase can catalyze reduction of a variety of other substrates including acetylene, azide, cyanide, isocyanide, and protons to hydrogen. [5, 8-10] Molybdenum nitrogenase is the most studied type of nitrogenase mainly expressed by diazotrophs. It consists of two main components: a catalytic component called MoFe protein, and a reductase component called iron protein. [4, 5] Molybdenum nitrogenase houses three types of metallocofactors which are some of the most complex ones found in the nature. Figure 1.2 represents the structure of Mo nitrogenase from *A. vinelandii.*
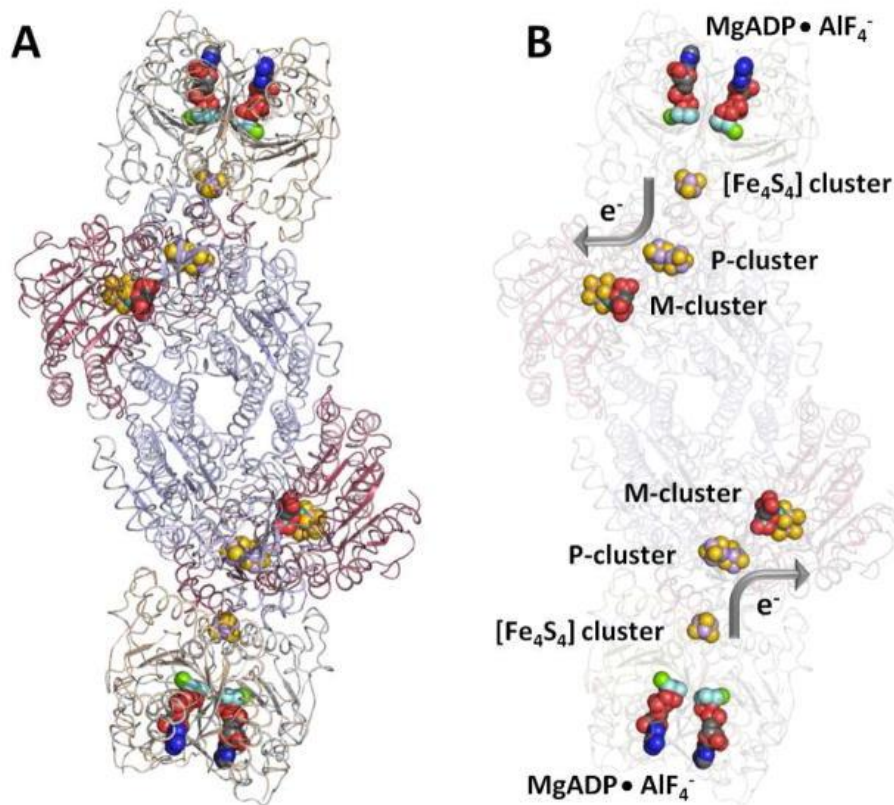
Figure 1.2 Crystal structure of the ADP·AlF₄−stabilized NifH/NifDK complex (A) and the relative positions of components involved in the transfer of electrons (B). The two subunits of NifH are colored gray and light brown, and the α- and β-subunits of NifDK are colored red and light blue, respectively, in (A). The same subunits are rendered transparent in the background in (B). All clusters and ADP·AlF₄⁻ are shown as space-filling models. Atoms are colored as follows: Fe, light purple; S, gold; Mo, brown; O, red; C, dark gray; N, dark blue; Mg, green; Al, beige; F, light blue. PYMOL was used to create this figure (PDB ID: 1N2C). [12]

1.2 Reductase Component

Reductase component is called dinitrogenase reductase or commonly known as iron Protein (Fe-Protein) which is a homodimer (γ_2) coded by *nif*H gene. The iron protein is a ~60 kDa dimer with identical subunits housing a single [Fe₄S₄] cluster symmetrically ligated between two subunits and each subunit contributes to cysteine residues to the cluster (Cys97 and Cys132). [13] Each subunit consists of one nucleotide biding site located 15 Å away from [Fe₄S₄] cluster. Figure 1.3 represents the detailed structure of iron protein.
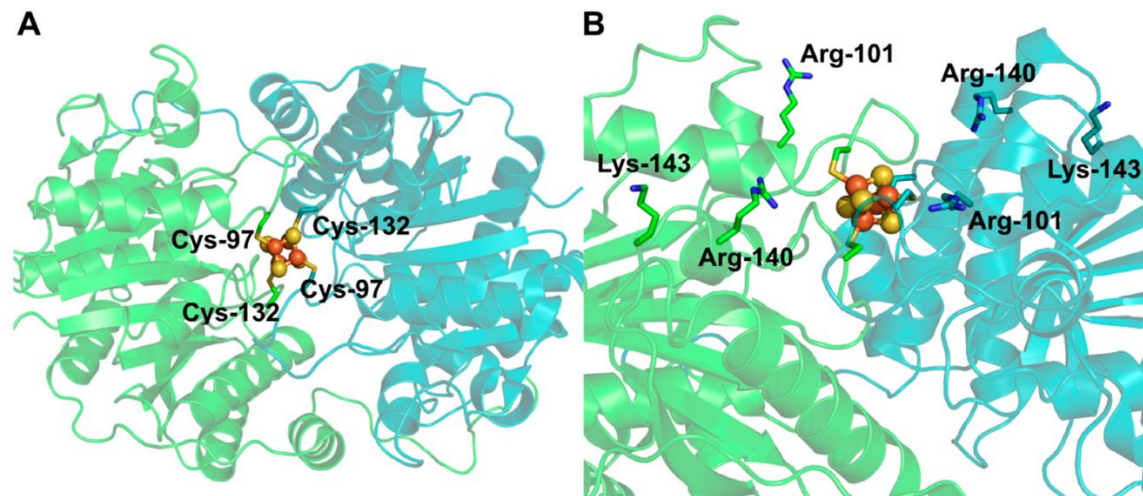
Figure 1.3 Crystal structure of NifH (PDB code 1G5P)- [14] Green and cyan ribbons represent the α and β subunits, respectively. **A**: representation of NifH as seen down the axis of symmetry. **B**: representation of NifH showing surface residues that have been identified as important for interactions with the MoFe protein. The Fe and S atoms of the [Fe$_4$S$_4$] cluster are shown as orange and yellow spheres, respectively. [15]

Iron protein has crucial roles in the nitrogen fixation process and metallocofactor assembly. Three primary functions are: 1. Insertion of Mo and homocitrate for M-cluster maturation; 2. Providing electron to the catalytic component for nitrogen fixation catalysis; 3. Facilitating P-cluster formation on NifDK. Moreover, it has been discovered that iron protein can reduce carbon monoxide and carbon dioxide to short chain hydrocarbons.

The [Fe$_4$S$_4$] cluster has the main role in the functions of iron protein. This cluster can occupy three different oxidation states: [Fe$_4$S$_4$]^0 known as all-ferrous state, [Fe$_4$S$_4$]$^{+1}$, and [Fe$_4$S$_4$]$^{+2}$. The functioning redox couple are thought to be the physiologically relevant pair of [Fe$_4$S$_4$]$^{+1}$ and [Fe$_4$S$_4$]$^{+2}$. [16, 17] The summary of the midpoint reduction potential (E$_m$) for iron protein of *A. vinelandii* is provided below.

$$[Fe_4S_4]^{+2} \quad \xrightleftharpoons{E_m = -290 \text{ mV}} \quad [Fe_4S_4]^{+1} \quad \xrightleftharpoons{E_m = -790 \text{ mV}} \quad [Fe_4S_4]^{0}$$
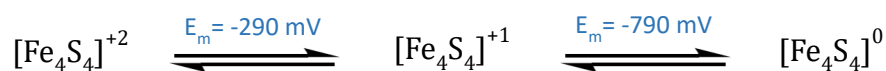
Former calorimetric chelation studies on iron protein from *A. vinelandii* had confirmed that the [Fe$_4$S$_4$] cluster is more accessible in the presence of MgADP, and it could easily be extracted by chelating agents such as bathophenanthrolinedisulfonate and 2,2'-bipyridine. This indicated that the binding of MgADP or MgATP could induce some conformational changes to the iron protein structure leading to a more solvent expose [Fe$_4$S$_4$] cluster. Discovery of crystal structures of iron protein has confirmed such theory and proved that in the presence of MgATP and MgADP, there is rather a significant rearrangement in the structure of iron protein from *A. vinelandii*. [18-21] Overlaying the crystal structures of iron protein with and without MgADP reveals a ~3 Å displacement of [Fe$_4$S$_4$] cluster, meaning upon MgADP binding to the iron protein, the cluster is more surface-exposed to facilitate the electron transfer (ET) to the catalytic component (MoFe protein), after cleavage of MgATP the recession of [Fe$_4$S$_4$] cluster prevents electron backflow. [15, 22] Rearrangement of iron protein structure and ~3 Å displacement of [Fe$_4$S$_4$] cluster upon MgATP and MgADP binding are depicted by overlaying crystal structure of iron protein docked to the catalytic component (NifDK or MoFe) and shown in Figure 1.4.
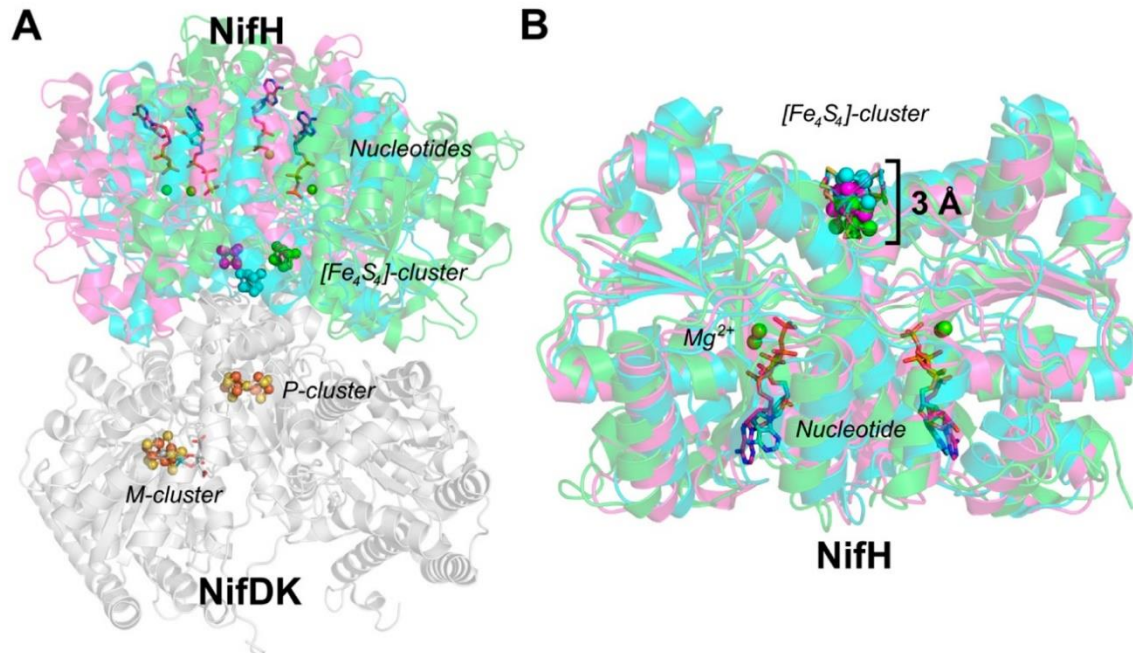
Figure 1.4 Overlaid crystal structure of NifH:NifDK complex with various nucleotides bound.
A: The NifDK protein (gray, PDB code 2AFH) in complex with NifH (green, PDB code 2AFH), MgADP-bound NifH (purple, PDB code 2AFI) and MgATP-bound ΔL127-NifH (cyan, PDB code 1G21). **B:** The aligned crystal structures of the NifH proteins from the NifH:NifDK complexes represented in panel A. The [Fe$_4$S$_4$] clusters of NifH are shown as spheres of the same color as the cartoon. The nucleotides are represented in a stick model; Mg atoms are shown as light green spheres. [15]

1.3 Catalytic Component

Catalytic component of nitrogenase from *A. vinelandii* is the most studied and best characterized nitrogenase system. Molybdenum nitrogenase (Mo nitrogenase) is a heterotetrametric α$_2$β$_2$ coded by nifD and nifK genes and is ~230 kDa in size and houses two of the most complex metalloenzymes found in the nature. Each αβ-dimer contains a [Fe$_8$S$_7$] cofactor known as P-cluster and a [MoFe$_7$S$_9$C-(R-homocitrate)] complex known as M-cluster. M-cluster is ligated by three cysteine residues from each subunit (Cysα62, Cysα88, Cysα154, Cysβ70, Cysβ95, and Cysβ153) and is located at the αβ interface about 10 Å below the protein surface. [23, 24] Figure 1.5 shows the detailed structure of MoFe from *A. vinelandii* crystal.

8
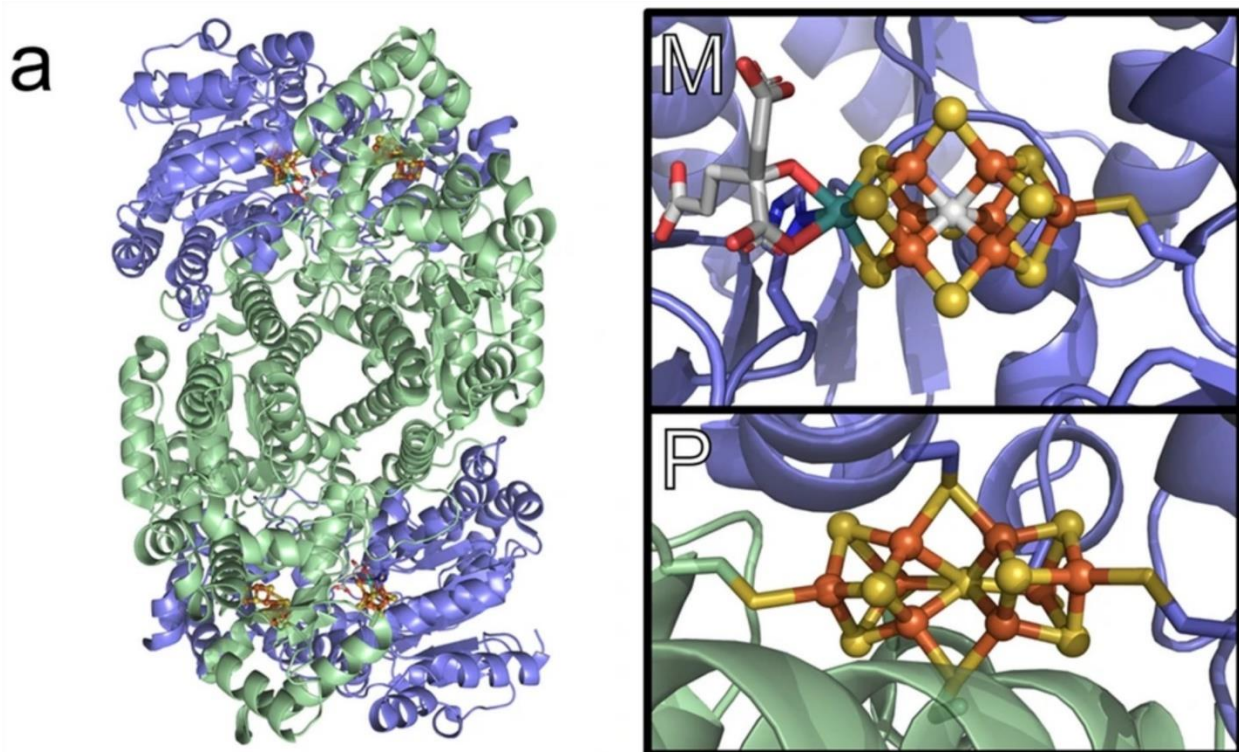
Figure 1.5 a: MoFe proteins of Mo nitrogenase and corresponding metallocofactors: M-cluster (FeMoco), P-cluster. The α-subunit of MoFe is displayed in blue, while the β-subunits are displayed in green (PDB 3U7Q) [25,26]

P-cluster shuttles electrons to M-cluster and the substrate turnover occurs on M-cluster, although the mechanism is yet to be discovered.

1.4 Specific Aims of Dissertation

The primary goal of this dissertation is to create a library of iron protein homologs in *E. coli* to be used as a toolbox for mechanistic investigations and to facilitate the heterologous expression of functional nitrogenase-based systems. To create such library, homologs of iron protein must be heterolougsly expressed in *E. coli*, grown, purified, and characterized using various methods which will be discussed in detail in chapter 2. Chapter 3 is focused on the

study of [Fe$_4$S$_4$] cluster and its unique characteristics. The latest chapter provides a brief overview of the expression of NifDK protein in *E. coli.*

CHAPTER 2

Heterologous Expression, Purification, and Characterization of Iron Proteins

2.1 Introduction

Nitrogenase is a key enzyme in the global nitrogen cycle [9, 16] produced by a certain types of soil bacteria (e.g., *Azotobacter vinelandii*), cyanobacteria (blue-green algae), and green sulfur bacteria. This enzyme carries out the ambient conversion of nitrogen (N_2) gas to ammonia (NH_3), as well as other reactions such as the conversion of acetylene (C_2H_2) and carbon monoxide (CO) to alkanes and alkenes. [9, 27-31] There are two major research directions in the study of the nitrogenase system 1) understanding the structure and function of the enzyme as well as its complex metallocofactors to better understand N_2 reduction and hydrocarbon formation and 2) the heterologous expression of the nitrogenase operon into different microorganisms for the development of microbe-based bioreactors and other biotechnology applications. The former research direction has been the focus of intense study for the past several decades, however, efforts to heterologously express nitrogenase proteins in different host organisms have been unsuccessful. In the bacterium *Azotobacter vinelandii*, nitrogenase facilitates the described chemistry through a two-component protein system (Figure 2.1).
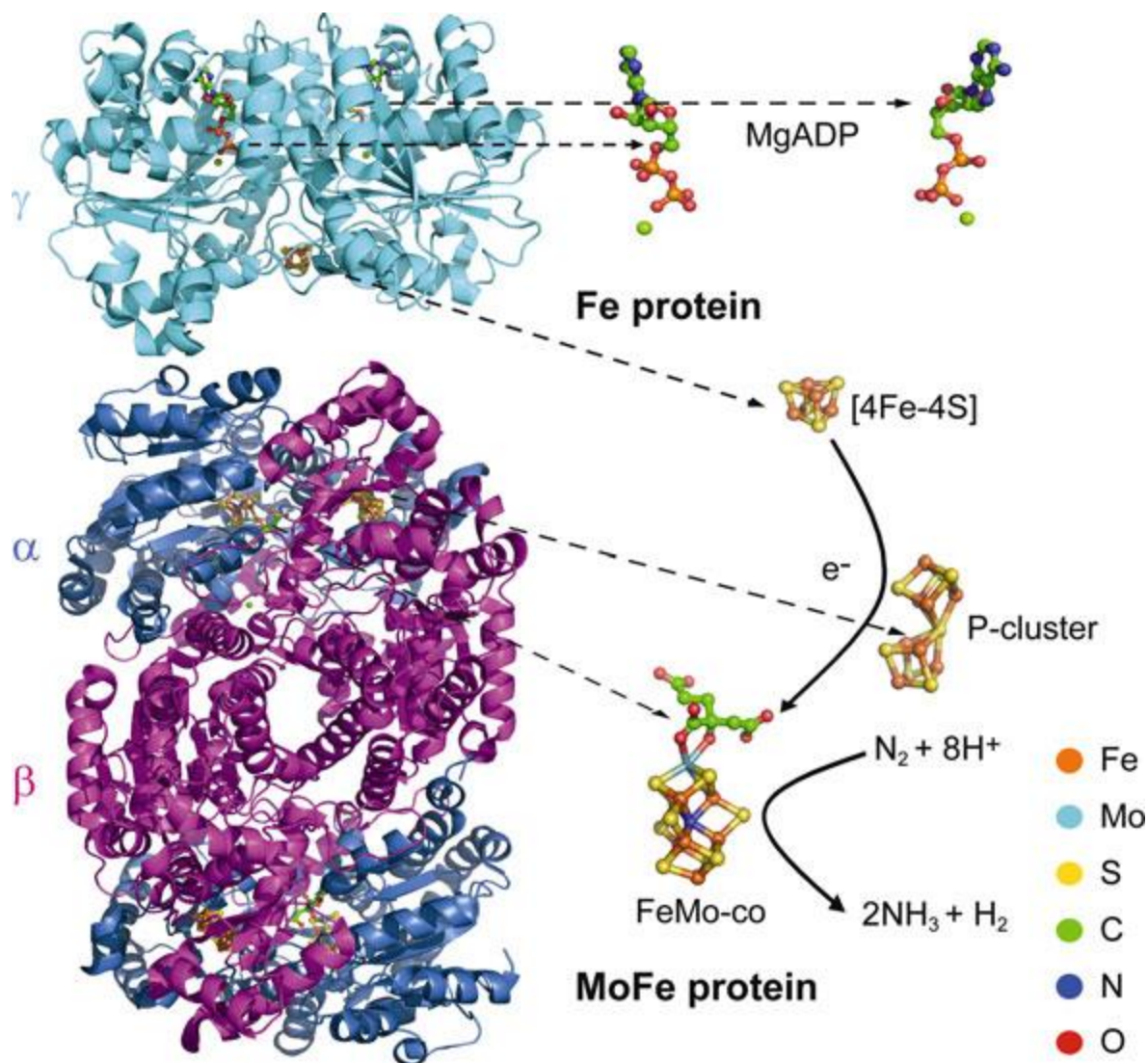
Figure 2.1 Crystal structure of the Fe and MoFe protein components of Mo-dependent nitrogenase showing the nucleotides, metal clusters, and electron transfer pathways. (Left) Representation of MoFe protein (PDB code 1M1N) with the α-subunits and the β-subunits and Fe protein (PDB code 1FP6) with the γ-subunits. (Right) Structures of MgADP and the three metalloclusters of nitrogenase. [32]

The catalytic component, called the MoFe protein or NifDK, where substrate reduction occurs, and the reductase component, called the iron protein or NifH, that houses a $[Fe_4S_4]$ cluster that transfers electrons during catalysis to the catalytic component and assists in the biosynthesis of the cofactors on NifDK. NifDK has two large FeS clusters, the $[Fe_8S_7]$ unit

called the P-cluster and the [MoFe$_7$S$_9$C(*R*-homocitrate)] unit called the M-cluster (Figure 2.2) that facilitate electron transfer as well as substrate binding and reduction. [12, 33-38]
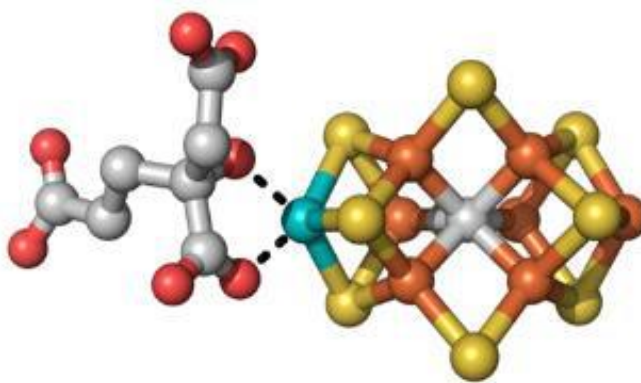
Figure 2.2 Model of M-cluster coordinated to (R)-homocitrate (C$_7$H$_8$O$_7$).
Colors of atoms: Fe = orange, S = yellow, C = gray, O = red, Mo = cyan. (PDB code 1N2C) [12]

The catalytic cycle in Mo-nitrogenase involves formation of a transient complex between NifH and NifDK, while the electron transfers from the [Fe$_4$S$_4$] cluster of NifH to the M-cluster, via the P-cluster, in NifDK. [12] The FeS cluster of the reductase component is unusual as it can support three known cluster oxidation states, (2+, 1+, and 0) whereas other FeS proteins cycle between only two states, and this cluster has also been found to convert CO and CO$_2$ to hydrocarbons in the absence of the catalytic component. [38-41] Due to these unique capabilities and the preliminary results from the previous work on *Methanosarcina acetivorans* (*M. acetivorans*), NifH has been selected as a target for studying and potentially modulating the protein-protein interactions and electron transfer between enzymatic components. [42]

As mentioned above, the heterologous expression of nitrogenase proteins has largely been unsuccessful, however, recently the Hu group was able to express NifH from the methanogenic organism *M. acetivorans* in *Escherichia coli (E. coli)* for the first time. [41] The

expression of the Fe protein in a non-diazotrophic system like *E. coli* provides the opportunity to more easily modify and express proteins that would otherwise be difficult, or impossible to accomplish in the native systems due to complex genetics and growth conditions of the organism. There is also a benefit of having access to a library of Fe proteins that could be studied in combination with other nitrogenase components, such as the catalytic component, to accomplish the expression of a functioning nitrogenase system in a heterologous host. As it is impossible to predict whether a nitrogenase gene component from one organism can be expressed in a heterologous non-diazotrophic system, it may be necessary to mix-and-match genes from a variety of diazotrophic organisms. Methanogenic organisms have demonstrated the ability to encode for Mo-nitrogenase homologs, however, these archaeal microorganisms are distinct from *A. vinelandii.* [37] The presence of these specific genes in methanogens makes them the perfect target for the investigation of the cross-reactivity of iron protein homologs with catalytic component of *A. vinelandii* (*Av*NifDK). Theoretical docking models have been employed to predict how well Fe protein homologs may interact with *Av*NifDK. [38, 43, 44] According to these calculations, the mean binding energy of the different protein conformations correlate with catalytic activity of the NifH:*Av*NifDK complex. In this work, additional Fe protein homologs (Table 2.1) were selected for heterologous expression in *E. coli* and characterized according to their predicted ability to interact with *Av*NifDK. The experimental activities will be compared to those predicted by the model to determine the effectiveness of the calculations.

Table 2.1 The Fe protein homologs, protein designations, and specificity markers. All the proteins were heterologously expressed in *E. coli* except *A. vinelandii* (*Av*NifH does not express in *E. coli*)

Organism	Abbrev.	Specificity Marker
Azotobacter vinelandii (*A. vinelandii*)	*Av*NifH	-14
Methanosarcina acetivorans (*M. acetivorans*)	*Ma*NifH	-6
Methanococcus maripaludis (*M. maripaludis*)	*Mmp*NifH	-7.8
Chlorobium phaeobacteroides (*C. phaeobacteroides*)	*Cp*NifH	-6.3
Geobacter uraniireducens (*G. uraniireducens*)	*Gu*NifH	-19.7
Methanosphaerula palustris (*M. palustris*)	*Mp*NifH	-8.6
Desulfovibrio vulgaris (*D. vulgaris*)	*Dv*NifH	-7.7

2.2 Experimental Methods

Unless noted otherwise, chemicals and reagents were obtained from Fisher Scientific or Sigma-Aldrich. All protein work was performed under Ar gas at an O_2 concentration of less than 5 ppm.

2.2.1 Cell Growth and Protein Purification

His-tagged MoFe protein (designated as *Av*NifH) expressed by *Azotobacter vinelandii* strains was grown and purified using previously reported methods. [45-47] Cells were grown in 180 L batches in a 250 L fermenter (New Brunswick Scientific) in Burke's minimal media containing 2 mM ammonium acetate, 4.6 mM K_2HPO_4, 1.5 mM KH_2PO_4, 0.8 mM $MgSO_4$, 3.4 mM NaCl, 0.3 mM $CaSO_4$, 0.01 mM Na_2MoO_4, 0.05 mM $FeSO_4$, and 2% sucrose (w/v). Cells were grown overnight, and the growth rate was monitored by optical density measurements at 436 nm using a Spectronic 20 Genesys spectrometer (Spectronic Instruments). After reaching a cell density of about 1.0, cells were harvested by flow-through centrifuge (Cepa)

then was mixed with 50 mM Tris-HCl (pH 8.0) and frozen. His-tagged Mo-nitrogenase *nifH*-encoded proteins from *Methanosarcina acetivorans, Methanococcus maripaludis, Chlorobium phaeobacteroides, Geobacter uraniireducens, Methanosphaerula palustris,* and *Desulfovibrio vulgaris;* designated as *Ma*NifH strain YM135EE, *Mmp*NifH strain YM218EE, *Cp*NifH strain YM221EE, *Gu*NifH strain YM222EE, *Mp*NifH strain YM220EE, and *Dv*NifH strain YM224EE, respectively; were grown in 40 L batches in a 80 L fermenter (New Brunswick Scientific) in Difco LB medium containing 100 mg/ml ampicillin (BD Bioscience). The growth rate was monitored by optical density measurements at 600 nm using a Spectronic 20 Genesys spectrometer. When the cell density reached 0.9-1.0 the temperature was lowered to 25 °C before inducing by the addition of 25 μM IPTG (isopropyl β-D-1-thiogalactopyranoside). Expression of protein was continued for 16-20 h before harvesting the cell by centrifugation using Thermo Fisher Scientific Legend XTR centrifuge.

Buffers were degassed on a vacuum-argon dual manifold Schlenk line for one hour before use. Then 2mM $Na_2S_2O_4$ reductant was added to each buffer, followed by an additional 10 minutes of degassing under vacuum. Buffers were kept under argon atmosphere after degassing and during the purification process. Frozen cells were mixed with a 1:1 volumetric ratio of 50 mM Tris-HCl (pH 8.0) containing 10 μg/ml deoxyribonuclease and 500 mM NaCl. Cells were thawed under vacuum for 45 minutes, followed by addition of 2 mM $Na_2S_2O_4$ reductant. Using a 110 L capacity microfluidizer (M-110 L Microfluidics Corporation) cell were lysed twice under argon atmosphere. The lysate mixture was degassed for 30 minutes, then transferred into centrifuge tubes within a glovebox. The lysate mixture was centrifuged at 14,000 x g for 45 minutes at 4 °C. The supernatant was collected and loaded onto equilibrated Ni-Sepharose resin; washed with 40 mM imidazole in 50 mM Tris-HCl (pH 8.0)

and 250 mM NaCl. The supernatant was eluted with 250 mM imidazole in 50 mM Tris-HCl (pH 8.0) and 250 mM NaCl.

Untagged iron proteins (NifH) were purified by loading the flow-through mixture of Ni-Sepharose onto a Q-Sepharose column; washed with 50 mM Tris-HCl (pH 8.0) and eluted with 500 mM NaCl and 50 mM Tris-HCl (pH 8.0). The eluted mixture was loaded onto Sephacryl S-200 SF size exclusion column and ran overnight in 50 mM Tris-HCl (pH 8.0) with 100 mM NaCl. The NifH protein fractions were collected by monitoring the elution profile at 405 nm. The iron protein fraction was loaded onto Q-Sepharose column and eluted by NaCl gradient (100 mM to 500 mM).

Purified proteins were frozen as pellets in liquid nitrogen and stored in liquid nitrogen filled dewars.

2.2.2 SDS-PAGE Analysis

SDS-PAGE analysis was performed using a 4-15% Mini-PROTEIN TGX precast gel (BioRad). The gel was run at 200 V and 50 mA for 40 min in TGX running buffer and stained with Coomassie Brilliant Blue.
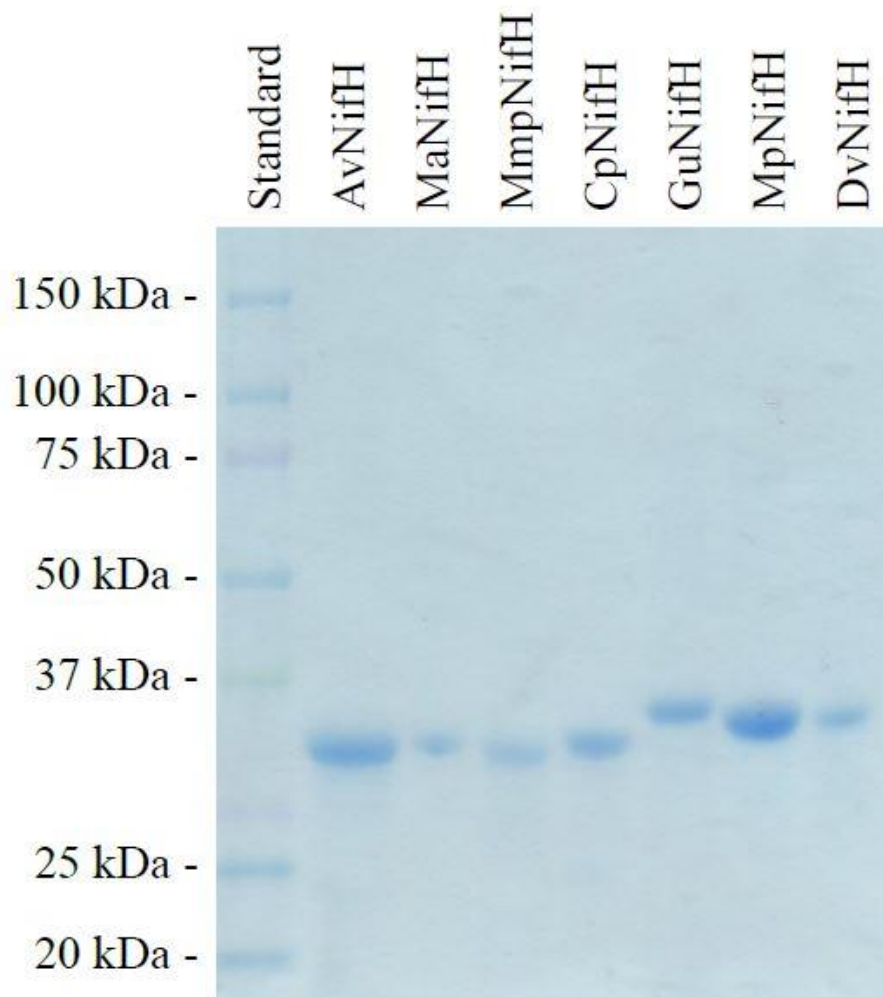
Figure 2.3 SDS-PAGE gel of iron protein homologs.

2.2.3 Iron Determination

The iron (Fe) content of the proteins was determined by inductively coupled plasma optical emission spectroscopy (ICP-OES) using a Thermo Scientific iCAP7000 instrument. Each protein was mixed with 200 µL 1:1 volumetric ratio of concentrated sulfuric acid (H_2SO_4) and nitric acid (HNO_3) and heated at 250 °C for 30 minutes. This procedure was repeated until the solutions became clear/colorless. The room temperate solutions were diluted with

19

2% HNO_3 (vol/vol) to a total volume of 7.5 mL and analyzed on the Thermo Scientific iCAP7000 instrument. [42]

2.2.4 EPR Analysis

Electron paramagnetic resonance (EPR) samples were prepared in a Vacuum Atmospheres glove box with less than 5 ppm O_2 and flash frozen in liquid nitrogen prior to analysis. [4] All the EPR samples contained 10 mg/mL pf purified protein; dithionite (DT)-reduced samples contained 25 mM Tris-HCl (pH 8.0), 250 mM imidazole, 10% (vol/vol) glycerol, 2 mM DT ($Na_2S_2O_4$). The DT-reduced samples were incubated with excess indigo disulfonate (IDS) for 5 minutes, followed by the removal of excess IDS using a G25 desalting column, resulting the IDS-oxidized samples. The all-ferrous samples were prepared by addition of 20 mM europium (II) diethylenetriaminepentaacetic acid (Eu^{II}-DTPA), followed by 5 minutes incubation and removal of excess Eu^{II}-DTPA using a G25 desalting column. EPR spectra were recorded by an ESP 300 E_z spectrophotometer (Bruker) interfaced with an ESR-9002 liquid-helium continuous-flow cryostat (Oxford Instruments) using 50 mW microwave power, a gain of 5×10^4, 100 kHz modulation frequency, 5 G modulation amplitude, at 10 K, and 9.62 GHz microwave frequency. [42]

2.2.5 Enzymatic Assays

The assay contained 0.27 mg of *Av*NifDK, 0.15 mg of iron protein homolog (*Mmp*NifH, *Cp*NifH, *Gu*NifH, *Mp*NifH, *Dv*NifH), 0.9 mM MgATP, 20 mM $Na_2S_2O_4$, 1.6 mM $MgCl_2$, 10 mM creatine phosphate, and 8 units creatine kinase (total volume of 1.0 mL). For N_2, CO, CO_2, C_2H_2, and H^+-reduction assays, 1 atm N_2, 1 atm CO, 1 atm CO_2, 0.1 atm C_2H_2, and 1 atm Ar were added to the headspace respectively. [27,35] Followed by 8 minutes incubation in 30 °C water bath. A

total of 250 µL of headspace was injected onto a Grace 5664PC column on a gas chromatograph-flame ionization detector (GC-FID, SRI 8610) for each assay. High purity helium was used as a carrier gas at 20 PSI. Determination of H_2, C_2H_4, and NH_3 were performed using the previously reported method. [12, 48]

2.2.6 M-cluster Maturation Assay

The assay contained 25 mM Tris-HCl (pH 8), 20 mM $Na_2S_2O_4$, 0.8 mM MgATP, 1.6 mM $MgCl_2$, 0.4 mM (*R*)-homocitrate, 10 mM creatine phosphate, 8 units creatine kinase, 0.4 mM molybdate (MoO^-_4), 0.3 mg Δ*nifB Av*NifDK, 1.3 mg Δ*nifHDK Av*NifEN, and 1.0 mg iron protein (total volume of 1 mL). The mixture was incubated at 30 °C water bath for 60 minutes, followed by determination of enzymatic activities according to previously reported methods. [42]

2.2.7 Docking Calculations

The affinity and specificity markers of nitrogenase complexes were defined using docking calculations and homology modeling using the previously reported methods. [42]

2.3 Results

2.3.1 Theoretical Docking Model

The homology modeling and *in silico* docking calculations were developed to predict the interaction of certain proteins to minimize the laborious, time-consuming, and expensive process of expression screening and purification of proteins. The theoretical docking calculation method was employed to screen the potential Mo-nitrogenase iron proteins and would allow us to predict the interactions of iron protein homologs with *Av*NifDK and

determine the electron flux for the nitrogenase hybrid systems. The "affinity marker" method was employed to choose the iron proteins from the pool of archaeal microorganisms for this investigation. Theoretical docking conformations of each iron protein homolog and the catalytic component hybrid were calculated using a previously reported method. [42]

2.3.2 Expression and Characterization of Iron Protein Homologs

Although challenging, the co-expression of iron protein homologs in *E. coli* with FeS assembly machinery (IscSUA) was successfully carried out. In order to increase the efficiency of protein expression, the source of iron (FeCl$_3$), in the growth phase was replaced by ferrous ammonium sulfate ($(NH_4)_2Fe(SO_4)_2 \cdot 6H_2O$) and the amount of IPTG (Isopropyl β-D-1-thiogalactopyranoside) was increased by three-fold to trigger transcription of the lac operon and induce the protein expression. All the iron protein homologs were purified on a Ni-sepharose affinity column. The protein purity was examined by SDS-PAGE (Figure S1) and the subunit size (≈30 kDa) was consistent with *Av*NifH that was purified according to the previously reported methods. [42, 47] Metal analysis was carried out, and the results for most of the homologs indicated >60% [Fe$_4$S$_4$] cluster occupancy is provided in Table 2.2.

Table 2.2 Metal analysis of the iron protein homologs.

Protein	# Fe / homodimer	% Occupancy
*Av*NifH	3.51 ± 0.10	88
*Ma*NifH	4.09 ± 0.11	102
*Mmp*NifH	3.37 ± 0.20	84
*Cp*NifH	3.98 ± 0.04	100
*Gu*NifH	6.75 ± 0.15	169
*Mp*NifH	2.65 ± 0.06	66
*Dv*NifH	2.52 ± 0.02	63

2.3.3 Characterization of the [Fe$_4$S$_4$] Cluster Using EPR Spectroscopy

In order to characterize the [Fe$_4$S$_4$] cluster of the iron protein homologs and compare them to the iron protein from *A. vinelandii*, EPR spectroscopy was performed, with the results summarized in Figure 2.4. The A, B, and C columns in Figure 2.4 correspond to the [Fe$_4$S$_4$] cluster in 2+, 1+ and 0 oxidation states, respectively. The 2+ oxidation state of [Fe$_4$S$_4$] cluster was achieved by addition of chemical oxidant indigo disulfonate (IDS), where the cluster exists in an $S = 0$ spin state and is EPR-silent. The cluster with a 1+ oxidation state exists as a mixture of S = 1/2 and S = 3/2 spin states, as purified in dithionite (Na$_2$S$_2$O$_4$, DT). The iron protein homologs in the 0+ oxidation state is called the "all-ferrous" $S = 4$ species, with a signal at $g = 15.9$ consistent with the iron protein from *A. vinelandii*. [36, 42]
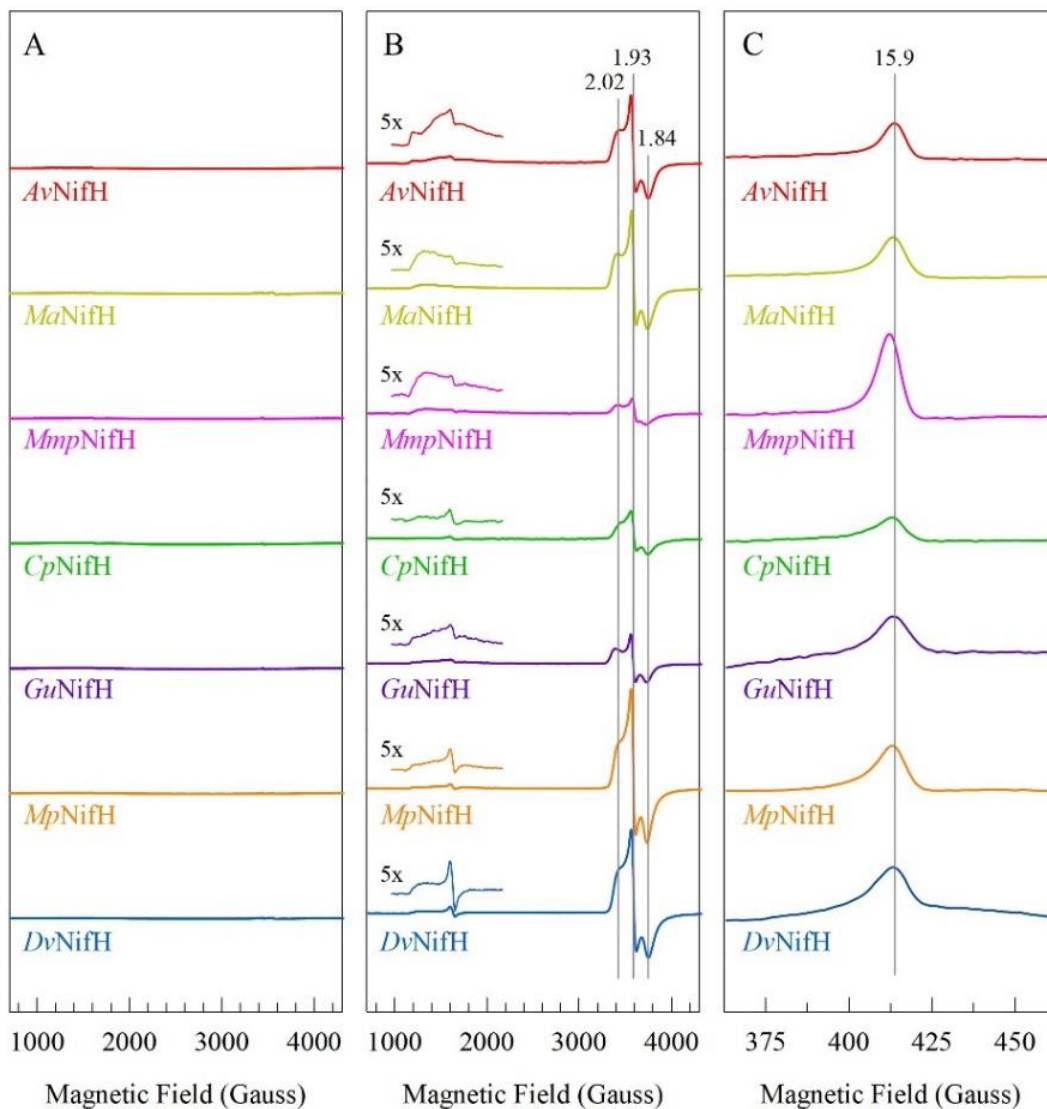
Figure 2.4 EPR spectra of iron protein homologs in IDS-oxidized ([Fe_4S_4]$^{2+}$, A), DT-reduced ([Fe_4S_4]$^{1+}$, B), and Eu^{II}-reduced all ferrous states ([Fe_4S_4]^0, C).

2.3.4 Cross-reactivities of the Iron Protein Homologs with *Av*NifDK

All the iron protein homologs were monitored for substrate reduction by four standard assays, N_2-, CO-, C_2H_2-, and H$^+$- reduction. The activities were calculated based on the nanomoles of electrons that appeared in the products per minute per milligram of iron protein, represented in Table 2.3.

Table 1.3 Interactions of the iron proteins with *Av*NifDK. Cross-reactivities of the iron protein homologs with *Av*NifDK were monitored by four standard substrates: N_2, CO, C_2H_2, and H^+. (HC = hydrocarbons)

	Activities (nmol electron min^{-1} mg^{-1})						
Substrate:	**N_2**		**CO**		**C_2H_2**		**H^+**
Product:	NH_3	H_2	HC	H_2	C_2H_4	H_2	H_2
***Av*NifH**	1650 ± 54	1185 ± 39	0.2 ± 0.7	2752 ± 4	2651 ± 54	120 ± 48	2793 ± 67
***Ma*NifH**	149 ± 19	121 ± 8	0.0 ± 0.5	332 ± 254	300 ± 1	72 ± 6	330 ± 37
***Mmp*NifH**	813 ± 6	571 ± 30	0.3 ± 0.2	1064 ± 109	1084 ± 66	44 ± 12	1216 ± 23
***Cp*NifH**	36 ± 13	49 ± 16	0.5 ± 0.3	104 ± 5	24 ± 0	25 ± 8	32 ± 3
***Gu*NifH**	0 ± 15	70 ± 11	0.3 ± 0.0	18 ± 1	20 ± 16	32 ± 20	120 ± 49
***Mp*NifH**	6 ± 3	53 ± 3	0.0 ± 0.1	75 ± 1	2 ± 1	20 ± 6	29 ± 10
***Dv*NifH**	964 ± 20	633 ± 17	0.0 ± 0.0	1205 ± 26	914 ± 25	28 ± 4	735 ± 117

2.3.5 M-cluster Maturation

Apart from the electron transfer to the catalytic component, iron protein plays a substantial role in both P-cluster biosynthesis and M-cluster assembly. [12] To this end, M-cluster maturation assay was performed to investigate the iron protein homologs ability to mature the precursor cluster, called the L-cluster, and determine their effectiveness in cofactor assembly (Table 2.4). Although, there is no apparent correlation between the N_2-reduction and M-cluster maturation; the iron protein interaction with *Av*NifDK during N_2-reduction and its interaction with *Av*NifEN for M-cluster maturation could explain such correlation.

Table 2.4 The comparative effectiveness of the Fe protein homologs to synthesize the M-cluster, represented as a percent to *Av*NifH.

	Relative M-cluster Formation (%)
*Av*NifH	100
*Ma*NifH	21.6
*Mmp*NifH	1.9
*Cp*NifH	7.8
*Gu*NifH	0
*Mp*NifH	0
*Dv*NifH	11.9

2.3.6 Non-native Reactivity

As mentioned before, the NifH reductase component can itself reduce CO and CO_2 to hydrocarbon products using Eu(II)-chelates as an electron source. [9, 27-31] The iron protein homologs expressed and purified in this study were similarly used to investigate potential CO and CO_2 reduction activity. The results of these reactions are summarized in Figures 2.5 and 2.6.
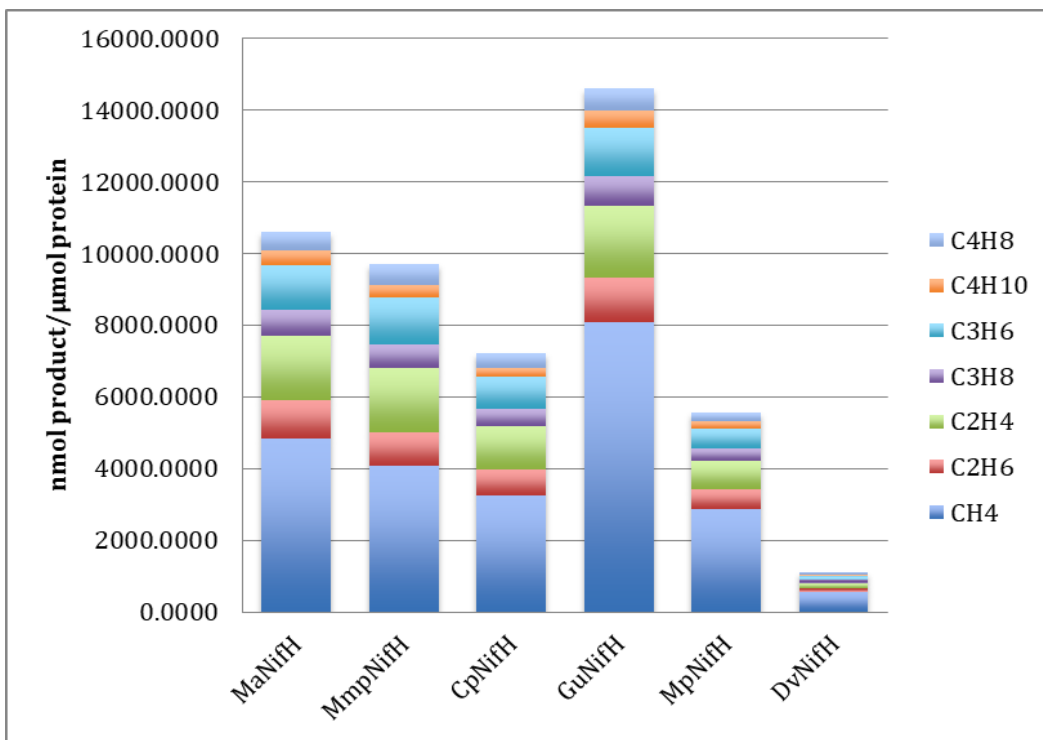
Figure 2.5 Reduction of CO by iron protein homologs to hydrocarbons.
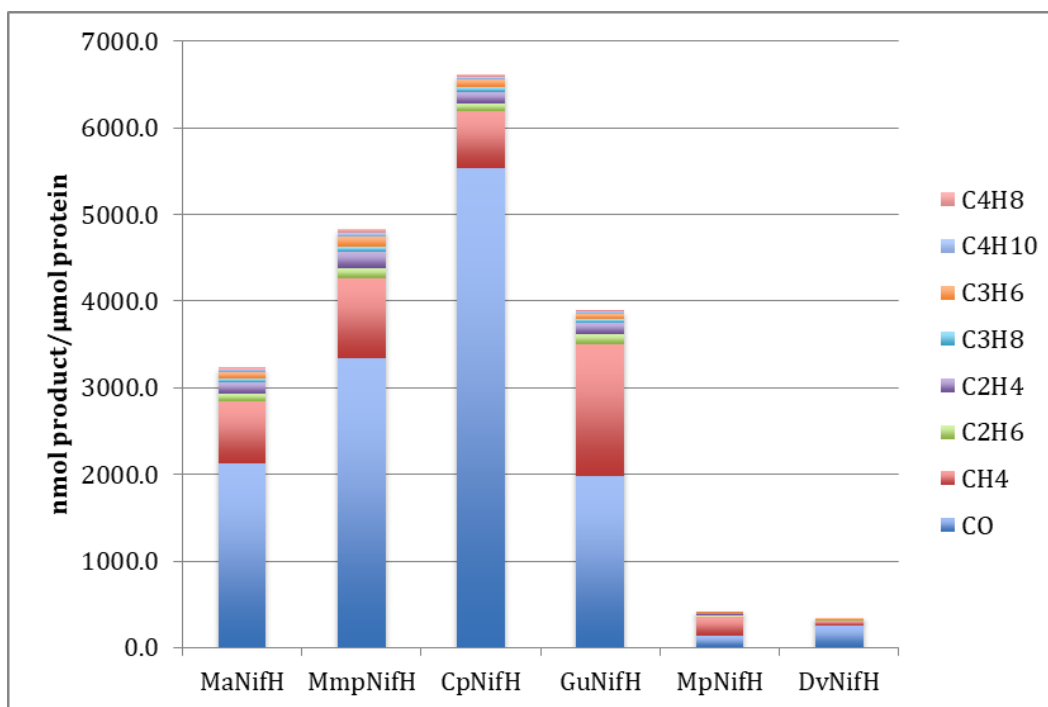
Figure 2.6 Reduction of CO$_2$ by iron protein homologs to CO and hydrocarbons.

2.4 Discussion

The metal analysis results of all of the iron protein homologs indicate that these proteins have >60% [Fe$_4$S$_4$] cluster occupancy, with the exception of *Gu*NifH, which has a much greater apparent Fe content (169% cluster occupancy). *Gu*NifH will be further purified to remove this adventitious iron that likely non-specifically binds to the protein. The *Mmp*NifH/*Av*NifDK and *Dv*NifH/*Av*NifDK hybrid systems reflect the highest catalytic activities while the lowest activities (≈ 2% activity compared to *Av*NifH/*Av*NifDK) were observed in the *Cp*NifH/*Av*NifDk, *Gu*NifH/*Av*NifDK hybrids. Among all the selected iron protein homologs, *Gu*NifH and *Mp*NifH were found to be ineffective in M-cluster maturation, while *Ma*NifH and *Dv*NifH represent the highest M-cluster maturation activity compared to the native *A. vinelandii* iron protein. Based on EPR spectroscopic analysis, the $S = 1/2$ rhombic signal of the Fe proteins is predominantly featured, and comparable to the same signal in *Av*NifH. The homologs also show the all-ferrous $S = 4$ signal at $g = 15.9$ which is consistent with the iron protein from *A. vinelandii,* but the intensities of the signals are not equivalent, which could be interesting criteria for further investigations.

2.5 Conclusion and Future Work

In this work, progress has been made towards expression and characterization of five additional Mo-nitrogenase iron proteins in a heterologous host. The metal analysis data indicates that the homologs all have >60% cluster occupancy. All of the iron protein homologs were reacted with *Av*NifDK using four standard substrate reduction assays (N$_2$, CO, C$_2$H$_2$, and H$^+$) and were shown to be functional hybrid nitrogenase systems. EPR spectroscopy demonstrated the ability of the [Fe$_4$S$_4$] cluster to adopt three oxidation states as-isolated, without requiring a reconstitution step, greatly simplifying purification. The

diversity of the all-ferrous $S = 4$ signal at $g = 15.9$ potentially indicates a difference in redox potential in the homologs that can be explored in future studies. Although *Dv*NifH was shown to be the most active homolog for N_2-, C_2H_2, and H^+ reduction, this protein did not produce any hydrocarbons in the CO reduction assay. This difference could potentially be exploited for future structure/function investigations. *Mmp*NifH shows a high cross-reactivity with *Av*NifDK, while being quite inactive for the M-cluster maturation. These properties of *Mmp*NifH may provide an opportunity to study and trap cluster intermediates during the biosynthesis of NifDK. Additionally, as the hybrid cross-reactivity assays showed that *Mmp*NifH and *Dv*NifH have the highest substrate reduction capability when paired with *Av*NifDK, these proteins would be excellent candidates for the heterologous co-expression of a functional nitrogenase-based system in *E. coli*.

CHAPTER 3

Probing the All-Ferrous States of Methanogen Nitrogenase Iron Proteins

3.1 Introduction

The Fe protein of nitrogenase reduces two C1 substrates, CO_2 and CO, under ambient conditions when its $[Fe_4S_4]$ cluster adopts the all-ferrous $[Fe_4S_4]^0$ state. Here, we show disparate reactivities of the nifH- and vnf-encoded Fe proteins from *Methanosarcina acetivorans* (designated *MaNifH* and *MaVnfH*) toward C1 substrates in the all-ferrous state, with the former capable of reducing both CO_2 and CO to hydrocarbons, and the latter only capable of reducing CO to hydrocarbons at substantially reduced yields. EPR experiments conducted at varying solution potentials reveal that *MaVnfH* adopts the all-ferrous state at a more positive reduction potential than *MaNifH*, which could account for the weaker reactivity of the *MaVnfH* toward C1 substrates than *MaNifH*. More importantly, *MaVnfH* already displays the g = 16.4 parallel-mode EPR signal that is characteristic of the all-ferrous $[Fe_4S_4]^0$ cluster at a reduction potential of −0.44 V, and the signal reaches 50% maximum intensity at a reduction potential of −0.59 V, suggesting the possibility of this Fe protein to access the all-ferrous $[Fe_4S_4]^0$ state under physiological conditions. These results bear significant relevance to the long-lasting debate of whether the Fe protein can utilize the $[Fe_4S_4]^{0/2+}$ redox couple to support a two-electron transfer during substrate turnover which, therefore, is crucial for expanding our knowledge of the reaction mechanism of nitrogenase and the cellular energetics of nitrogenase-based processes

The iron sulfur (FeS) proteins play crucial roles in biological processes that range from iron homeostasis and gene regulation to electron transfer and enzyme catalysis. [16, 49-52] A member of the FeS protein family, the iron (Fe) protein is the reductase component of nitrogenase, a key enzyme in the global nitrogen cycle that catalyzes the ambient reduction

of the atmospheric N_2 to the bioavailable NH_3. Encoded by nif H and vnfH, respectively, the Fe proteins of Mo- and V-nitrogenases (designated NifH and VnfH) are structurally homologous homodimers that house a surface-exposed [Fe_4S_4] cluster at the subunit interface and an MgATP-binding site within each subunit. During substrate turnover, NifH or VnfH forms a functional complex with its catalytic partner, NifDK or VnfDGK, which allows electrons to be transferred concomitantly with ATP hydrolysis from the [Fe_4S_4] cluster of the former, via a so-called P- or P*-cluster, to the M- or V-cluster (generally termed the cofactor) of the latter, where substrate reduction takes place (Figure 3.1a). [52-55] Other than serving as an obligate electron donor for its catalytic partner in the complete nitrogenase enzyme system, the Fe protein can act as a reductase on its own and catalyze the ambient reduction of CO_2 and CO (Figure 3.1b). [40, 56, 57]
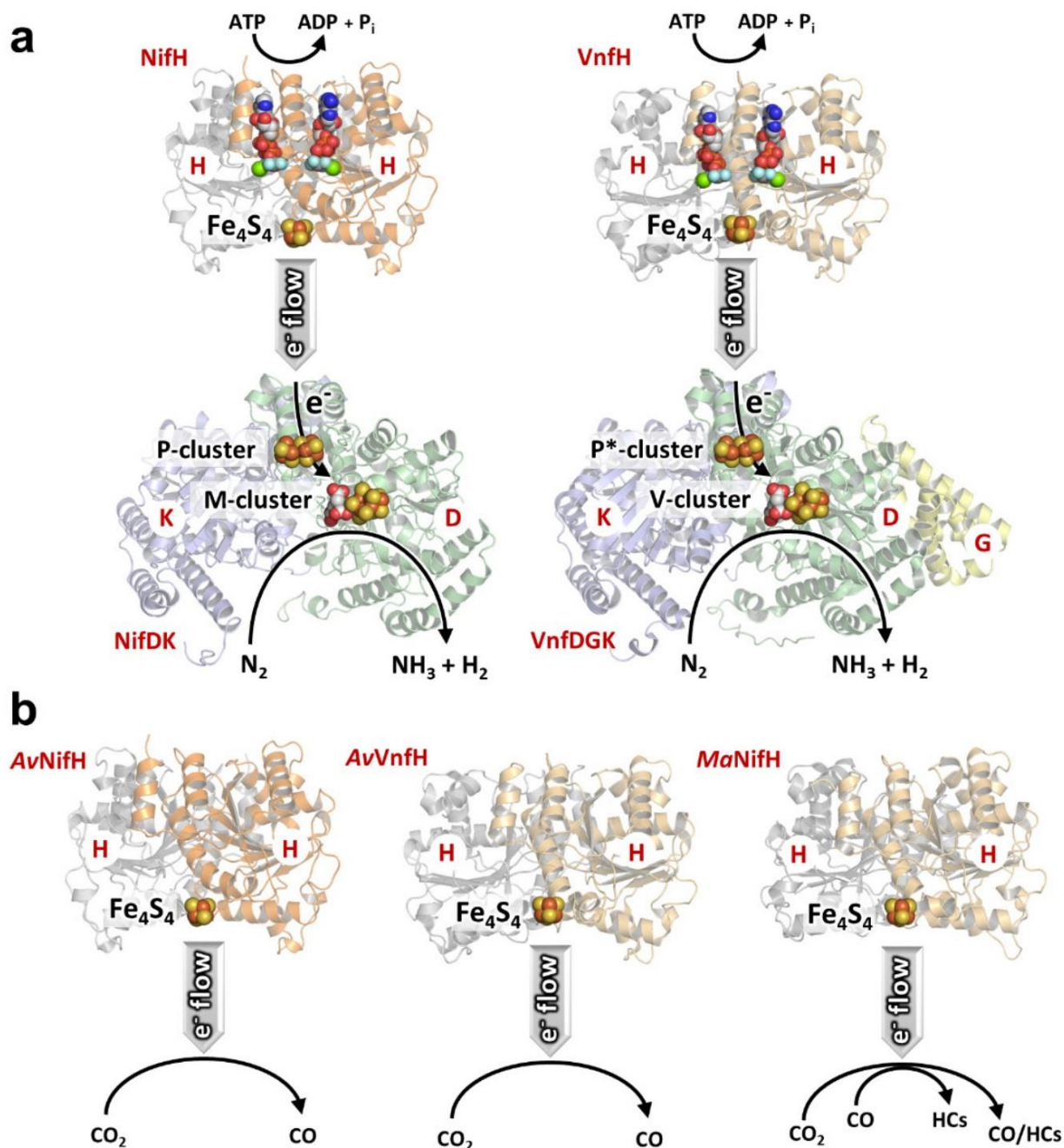
Figure 3.1 Functions of Fe protein (a) as an electron donor to its catalytic partner to enable nitrogenase catalysis or (b) as an independent reductase of C1 substrates. (a) Catalysis by the Mo- (left) or V- (right) nitrogenase, which involves transfer of electrons from the $[Fe_4S_4]$ cluster of the Fe protein (NifH or VnfH), via the P- or P*-cluster, to the M- or V-cluster of the catalytic partner (NifDK or VnfDGK), where substrate reduction takes place. (b) Catalysis by the nucleotide-free NifH or VnfH as an independent reductase of C1 substrates. The NifH (left) and VnfH (right) proteins from Azotobacter vinelandii (designated AvNifH and AvVnfH, respectively) can reduce CO_2 to CO; whereas the NifH protein from Methanosarcina acetivorans (designated MaNifH) can reduce CO2 and CO to hydrocarbons. The subunits of the Fe proteins are colored yellow and orange, the subunits of the

catalytic partners are colored light green, light blue, and yellow. Atoms are colored as follows: Fe, orange; S, yellow; C, gray; Mo, teal; V, dark gray; O, red; N, blue; P, tangerine; Mg, green; Al, light blue. PDB entries 1N2C, [23] 5N6Y, [57] 6Q93, [58] and 6NZJ [59] were used to generate this figure.

The reactivity of Fe protein toward C1 substrates was first observed in *Azotobacter vinelandii*, a soil bacterium, where both NifH and VnfH proteins of this microorganism were shown to reduce CO_2 to CO under in vitro or in vivo conditions.10 Subsequently, the NifH protein of a methanogenic organism, *Methanosarcina acetivorans*, was demonstrated to reduce CO_2 and CO to hydrocarbons under in vitro conditions. [60] These observations have established the Fe protein as a simple FeS enzyme that is capable of generating hydrocarbons via reactions that resemble the Fischer–Tropsch (FT) process [61] that is used for the industrial production of carbon fuels; however, unlike the FT process, the reactions catalyzed by the Fe protein utilize protons/electrons (instead of H_2) as the reducing power, and they occur at ambient temperature and pressure. The ability of the Fe protein to serve as a reductase relies on the redox versatility of its $[Fe_4S_4]$ cluster, which can reversibly adopt at least three oxidation states: the super-reduced, all-ferrous state ($[Fe_4S_4]^0$); the reduced state ($[Fe_4S_4]^{1+}$); and the oxidized state ($[Fe_4S_4]^{2+}$). [16, 48] The ability of the Fe protein to adopt the all-ferrous state makes it unique among the $[Fe_4S_4]^-$ cluster-containing proteins that are usually confined to two oxidation states other than the super-reduced state, [62] although it is unclear whether the all-ferrous state can be reached by the Fe protein under physiological conditions. Nevertheless, while it is generally believed that the $[Fe_4S_4]^{1+/2+}$ redox couple is used by the Fe protein for a one-electron transfer to its catalytic partner during nitrogenase catalysis, it has been suggested that the Fe protein could also use the $[Fe_4S_4]^{0/2+}$ couple for a two-electron transfer in this process. Likewise, the reduction of CO_2 and/or CO by the Fe protein on its own is best achieved in the presence of europium(II) diethylene-

triaminepentaacetic acid [Eu(II)-DTPA] ($E_{1/2}$ = −1.14 V at pH 8), [63] a strong reductant that renders the [Fe_4S_4] cluster of the Fe protein in the "super-reduced", all-ferrous [Fe_4S_4]^0 state. These observations have led to the question of whether the all-ferrous state of the Fe protein can be accessed at physiological reduction potentials achieved by the in vivo electron donors to this protein, such as ferredoxins and flavodoxins, to enable substrate reduction in the cell.

3.2 Experimental Methods

Unless noted otherwise, chemicals and reagents were obtained from Fisher Scientific or Sigma-Aldrich. All protein work was performed under Ar gas at an O_2 concentration of less than 5 ppm.

3.2.1 Cell Growth and Protein Purification

E. coli strains expressing His-tagged *MaNifH* (strain YM135EE) and *MaVnfH* (strain YM136EE) [42] were grown in 10-L batches in Difco LB medium containing 100 mg/L ampicillin (BD Biosciences) in a BIOFLO 415 fermenter (New Brunswick Scientific) at 37°C, with 200 rpm agitation and 10 L/min airflow. Growth rates were monitored by measuring cell density at 600 nm using a Spectronic 20 Genesys spectrometer (Spectronic Instruments). When OD_{600} reached 0.5, the temperature was lowered to 25°C before expression of *MaNifH* or *MaVnfH* was induced by addition of 25 μM IPTG. The *MaNifH* or *MaVnfH* protein was allowed to express for 16 h before cells were harvested by centrifugation using a Thermo Fisher Scientific Legend XTR centrifuge. Subsequently, His-tagged *MaNifH* or *MaVnfH* was purified by immobilized metal affinity chromatography (IMAC) using methods adapted from the purification of His-tagged nitrogenase proteins. [8, 64] Specifically, 80 g of cell paste was resuspended in a buffer containing 25 mM Tris-HCl (pH 8.0), 2 mM sodium dithionite, 1 mM

phenylmethylsulfonyl fluoride (PMSF) and 500 mM NaCl. The cell suspension was disrupted by a microfluidizer and centrifuged at 15,000 ×g to remove cell debris. The resultant, clear supernatant was loaded on a column packed with Ni sepharose 6 Fast Flow resin (~15 mL, GE Healthcare). Subsequently, the column was washed with a buffer containing 25 mM Tris-HCl (pH 8.0), 2 mM sodium dithionite, 500 mM NaCl and 40 mM imidazole, followed by elution of protein from the column with the same buffer containing 250 mM imidazole. The *MaNifH* and *MaVnfH* proteins were collected as dark brown eluents and subjected to further characterization.

3.2.2 EPR Analysis

The electron paramagnetic resonance (EPR) samples were prepared in a Vacuum Atmospheres glove box with less than 5 ppm O_2 and flash frozen in liquid nitrogen prior to analysis. The dithionite-reduced samples contained 10 mg/mL of *MaNifH* or *MaVnfH*, 25 mM Tris-HCl (pH 8.0), 10% (vol/vol) glycerol, 250 mM imidazole, and 2 mM or 20 mM sodium dithionite. The europium(II) compound-reduced samples were prepared by incubating the sample with 10 mM europium(II) 1,4,7,10-tetrakis(carbamoylmethyl)-1,4,7,10-tetraazacyclododecane [Eu(II)- DOTAM], 10 mM europium(II) 1,4,7,10-tetraazacyclododecane-1,4,7,10-tetraacetic acid [Eu(II)- DOTA), or 10 mM europium(II) diethylenetriaminepentaacetic acid [Eu(II)-DTPA] for 5 min, followed by removal of excess Eu(II) compound using a G25 desalting column. EPR spectra were recorded by an ESP 300 E_z spectrophotometer (Bruker) interfaced with an ESR-9002 liquid-helium continuous-flow cryostat (Oxford Instruments) using a microwave power of 50 mW, a gain of 5×10^4 , a modulation frequency of 100 kHz, and a modulation amplitude of 5 G. Five scans were

recorded for each EPR sample at a temperature of 10 K and a microwave frequency of 9.62 GHz.

3.2.3 Determination of Reduction Potentials of Eu(II)-DOTA and Eu(II)-DOTAM

The cyclic voltammetry measurements of Eu(II)-DOTAM and Eu(II)-DOTA were performed on a Pine Wavedriver 10 potentiostat with AfterMath software in a glove box filled with dinitrogen. The conditions used to measure the samples were as follows: sample concentration, 1 mM; solvent, 25 mM Tris-HCl buffer (pH 8.0); temperature, room temperature; working electrode, vitreous carbon disc (1-mm diameter); auxiliary electrode, vitreous carbon rod; reference electrode, saturated calomel electrode (SCE, CH Instruments); supporting electrolyte, 200 mM KCl; sweep speed, 0.1 V/sec. The solution samples were prepared by diluting the bright yellow solutions of Eu(II)-DOTA and Eu(II)-DOTAM at 100 mM to the final concentration of 1 mM in the Tris-HCl buffer (pH 8.0) that contained 200 mM KCl. The potentials referenced to the SCE were converted to values with reference to the standard hydrogen electrode (SHE) by the following equation: E (vs. SHE) = E (vs. SCE) + 244 mV. [65]

3.2.4 CO_2- and CO-reduction Assays

The in vitro CO_2- and CO-reduction assays were carried out in 9.4 mL assay vials with crimped butyl rubber serum stoppers. Each assay contained, in a total volume of 1.0 mL, 0.5 mg *MaNifH* or *MaVnfH*, increasing concentrations (10, 20, 40 or 100 mM; for CO_2-reduction assays) or 100 mM (for CO-reduction assays) of Eu(II)-DTPA, and either 500 mM Tris-HCl, pH 10 (for CO_2-reduction assays) or 250 mM Tris-HCl, pH 8 (for CO-reduction assays). The CO-reduction assays of *MaVnfH* were conducted in the presence of ^{12}CO or ^{13}CO. The

optimum concentration of CO_2 (100%) or CO (0.53%), which resulted in the maximum amount of product(s), was determined by titration with increasing concentrations of CO_2 or CO added to the headspace of the respective assay. The CO_2-reduction assays were assembled by repeatedly flushing and exchanging the buffer solution without Eu(II)-DTPA and protein with 100% CO_2, followed by equilibration for 30 min until pH stabilized at ~8.1; whereas the CO-reduction assays were assembled by repeatedly flushing and exchanging the buffer solution without Eu(II)- DTPA and protein with 100% Ar, followed by addition of 0.53% CO. The reaction was initiated by addition of *MaNifH* or *MaVnfH*, followed by immediate addition of Eu(II)-DTPA. The assay 4 mixture was then incubated with continuous shaking at 30°C until the reaction was complete (300 min), followed by quenching with 100 µL of 30% trichloroacetic acid. The headspace sample was subsequently examined for CO- and hydrocarbon-formation as described earlier. [60]

3.2.5 GC-MS Analysis

The products of ^{12}CO- and ^{13}CO-reduction by *MaVnfH* were analyzed by gas chromatography-mass spectrometry (GC-MS) using a Thermo Scientific Trace 1300 GC system coupled to a Thermo ISQ QD (Thermo Electron North America LLC). Specifically, a total of 250 µL headspace sample was injected into a split/splitless injector operated at 150°C in split mode with a split ratio of 10, followed by separation of gas on a HP-PLOT/Q+PT column (30 m × 0.32 mm ID × 20 µm film; Agilent Technologies North America LLC), which was held at 30°C for 3 min, heated to 200°C at a rate of 15°C/min, and held at 200°C for 5 min. The rate at which the carrier helium (He) gas passed through the column was held at 0.7 mL/min for 4 min, increased to 1.4 mL/min at a rate of 0.5 mL/min, and held at 1.4 mL/min for the

remainder of the run. The mass spectrometer was operated in the electron impact (EI) ionization mode. The fragmentation patterns of the products were compared to those of the C1-C4 alkane and alkene standards as described previously. [60]

3.3 Results and Discussion

To assess the all-ferrous state of the Fe protein, we first examined the utility of two Eu(II) chelates, europium(II)1,4,7,10-tetrakis(carbamoylmethyl)-1,4,7,10-tetraazacyclododecane [Eu(II)-DOTAM] and europium(II) 1,4,7,10-tetraaza-cyclododecane-1,4,7,10-tetraacetic acid [Eu(II)-DOTA], as potential reductants to probe the response of the all-ferrous state to varying solution potentials. The reduction potentials of Eu(II)-DOTAM and Eu(II)-DOTA were determined by cyclic voltammetry measurements of in situ generated complexes in 25 mM Tris-HCl buffer at pH 8.0. The resultant voltammograms (Figure 3.2) show the reversible Eu(III)/Eu(II) couples at $E_{1/2}$ = −0.59 V (for Eu(II)-DOTAM) and −0.92 V (for Eu(II)-DOTA) vs standard hydrogen electrode (SHE). These values are directly comparable with the reported potentials of Eu(II)-EGTA (−0.88 V vs SHE) and Eu(II)-DTPA (−1.14 V vs SHE) measured at pH 8.0. [63]
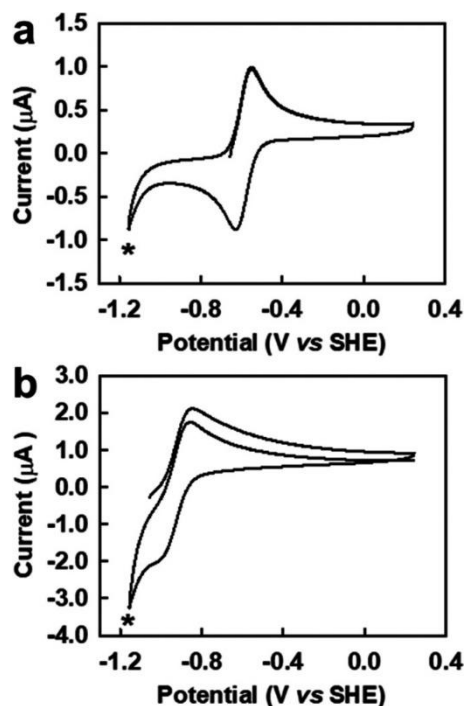
Figure 3.2 Cyclic voltammograms of (a) Eu(II)-DOTAM and (b) Eu(II)-DOTA in 25 mM Tris-HCl buffer at pH 8.0. The irreversible features, indicated by * at approximately −1.2 V, are attributed to the reduction of the solvent.

The fact that the potentials of Eu(II)-DOTAM and Eu(II)-DOTA are intermediate between those of dithionite (e.g., −0.47 V vs SHE at 2 mM, pH 8.0) [66, 67] and Eu(II)-DTPA makes them suitable candidates, together with the latter two reductants, for titrating the all-ferrous-specific EPR signal of the Fe protein versus solution potentials. With proper reductants identified for the titration experiment, we treated the NifH and VnfH proteins from *M. acetivorans* (designated *MaNifH* and *MaVnfH*) with 20 mM dithionite ($E_{1/2}$ = −0.44 V at pH 8.0), 2 mM dithionite ($E_{1/2}$ = −0.47 V at pH 8.0), 10 mM Eu(II)-DOTAM ($E_{1/2}$ = −0.59 V at pH 8.0), 10 mM Eu(II)-DOTA ($E_{1/2}$ = −0.92 V at pH 8.0), and 10 mM Eu(II)-DTPA ($E_{1/2}$ = −1.14 V at pH 8.0) and monitored the appearance of the all-ferrous state specific, g = 16.4 parallel-mode EPR signal at the various reduction potentials generated by these reductants. [48, 68]

Interestingly, despite sharing as high as 80% sequence homology, [42] *MaNifH* and *MaVnfH*

display distinct patterns of changes in the magnitudes of their all-ferrous-specific EPR

signals upon titration with the same set of reductants (Figure 3.2). In the case of *MaNifH*, the

g = 16.4 signal is hardly visible (1.1% of max. intensity) at −0.44 V, and it only becomes

apparent (14.8% of max. intensity) at −0.59 V (Figure 3.3a, b).
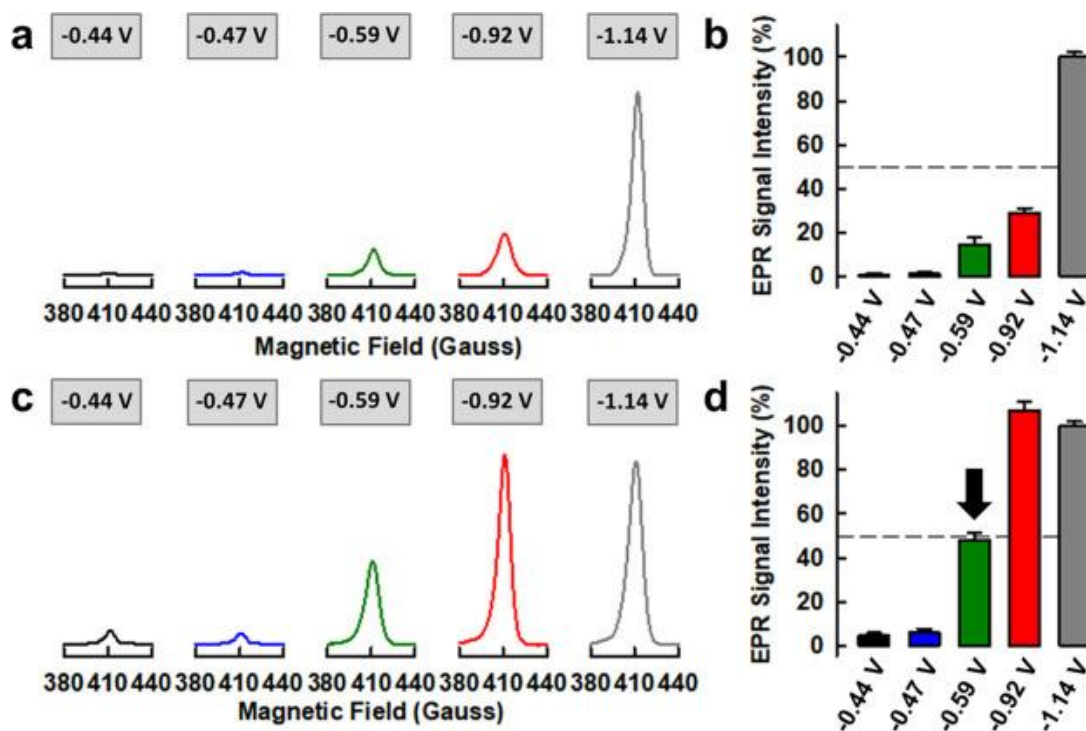

Figure 3.3 Titration of the all-ferrous-specific EPR signals of *MaVnfH* and *MaNifH* proteins versus solution potentials. (a, c) Appearance of the g = 16.4, parallel-mode EPR signal that is characteristic of the all-ferrous [Fe$_4$S$_4$] 0 cluster of *MaNifH* (a) and *MaVnfH* (c) in the presence of reductants with varying reduction potentials. The reductants used in this experiment were 20 mM dithionite ($E_{1/2}$ = −0.44 V at pH 8.0), 2 mM dithionite ($E_{1/2}$ = −0.47 V at pH 8.0), 10 mM Eu(II)-DOTAM ($E_{1/2}$ = −0.59 V at pH 8.0), 10 mM Eu(II)-DOTA ($E_{1/2}$ = −0.92 V at pH 8.0), and 10 mM Eu(II)-DTPA ($E_{1/2}$ = −1.14 V at pH 8.0). (b, d) Intensity of the g = 16.4 parallel-mode EPR signal versus the potential of the reductant used to generate the signal. The EPR signal intensity (%) was determined by double integration of the g = 16.4 signal and calculation of the relative intensity versus the maximum intensity at −1.14 V. The colored bars represent the EPR signal intensities (%) at $E_{1/2}$ = −0.44 V (black), $E_{1/2}$ = −0.47 V (blue), $E_{1/2}$ = −0.59 V (green), $E_{1/2}$ = −0.92 V (red), and $E_{1/2}$ = −1.14 V (gray). The EPR signal intensities (%) are 1.1 ± 0.5, 1.6 ± 0.3, 14.8 ± 3.2, 29.1 ± 2.2, and 100.0 ± 2.1, respectively, for *MaNifH*, and 4.7 ± 1.1, 5.9 ± 1.9, 48.0 ± 3.2, 107.3 ± 4.0, and 100.0 ± 2.2, respectively, for *MaVnfH*, at −0.44, −0.47, −0.59, − 0.92, and −1.14 V. The "midintensity" potential, or the potential corresponding to 50% of the maximum signal intensity, is indicated by a horizontal dashed line in parts b and d. For *MaNifH*, this value is ∼−0.59 V (part d, arrow).

In contrast, *MaVnfH* already displays a small, yet visible g = 16.4 signal (4.7% of max. intensity) at −0.44 V, and the signal (48% of max. intensity) is substantially stronger than that displayed by *MaNifH* (14.8% of max. intensity) at −0.59 V (Figure 3.2c,d). The appearance of the g = 16.4 signal in the spectrum of the dithionite-treated *MaVnfH* is surprising, as all Fe proteins characterized so far exist in the reduced $[Fe_4S_4]^{1+}$ state in the presence of dithionite and do not show the all-ferrous signal unless a lower potential is reached in the presence of a stronger reductant. For example, the $[Fe_4S_4]^{0/1+}$ couple of the NifH protein from *A. vinelandii* was determined to have a midpoint potential of −0.79 V.[20] In comparison, *MaVnfH* already reaches ~50% of the maximum intensity of the g = 16.4 signal at −0.59 V (Figure 3.3d, arrow), and it has a hue consistent with that right before conversion into the characteristic reddish-pink color of the all-ferrous state at this potential (Figure 3.4).
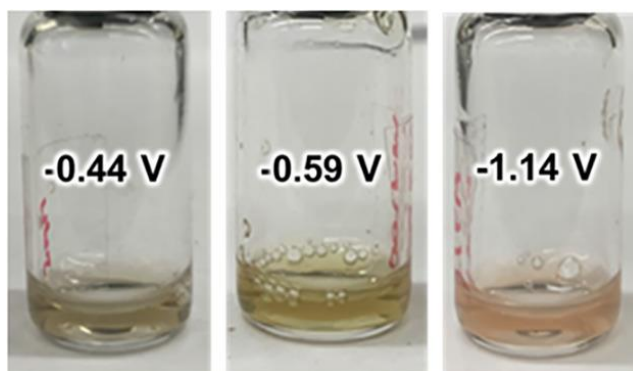
Figure 3.4 *MaVnfH* protein in 2 mM dithionite (left), 10 mM Eu(II)- DOTAM (middle), and 10 mM Eu(II)-DTPA (right). The $E_{1/2}$ values of the reductants are indicated.

As such, it is likely that the cluster of this Fe protein can access the all-ferrous $[Fe_4S_4]^0$ state under physiological conditions, where such a potential can be accomplished by certain ferredoxins as the electron donors to the Fe protein in the cell. [23, 70-72] The fact that *MaVnfH* adopts the all-ferrous state at a more positive reduction potential than *MaNifH* points to a

weaker ability of *MaVnfH* than *MaNifH* to donate lower-potential electrons to the C1 substrates in the all-ferrous state and, consequently, a weaker ability of the all-ferrous *MaVnfH* than its *MaNifH* counterpart to reduce these substrates. Indeed, we observed disparate reactivities of *MaNifH* and *MaVnfH* toward CO_2 and CO when these assays were conducted in the presence of Eu(II)-DTPA. In the case of *MaNifH*, both CO and hydrocarbons can be detected as products of CO_2 reduction, and the formation of CO (Figure 3.5a, left, black circles) decreases concomitantly with an increase in the formation of hydrocarbons (Figure 3.5a, right, black triangles) with increasing concentrations of Eu(II)-DTPA.

The maximum yields of CO (4.55 ± 0.19 nmol/nmol protein) and hydrocarbons (3.91 ± 0.32 nmol/nmol protein) are accomplished by *MaNifH* at 20 mM and 100 mM Eu(II)-DTPA, respectively. Contrary to *MaNifH*, *MaVnfH* shows no formation of CO (Figure 3.5a, left, blue circles) or hydrocarbons (Figure 3.5a, right, blue triangles) from CO_2 reduction under the same reaction conditions.

However, like *MaNifH*, *MaVnfH* can generate hydrocarbons from CO reduction when Eu(II)-DTPA is supplied at 100 mM (Figure 3.5b–d). The identities of the hydrocarbon products generated by *MaVnfH* (Figure 3.5b, lower), as confirmed by gas chromatograph–mass spectrometry (GC-MS) (Figure 3.5d), are the same as those generated by *MaNifH* (Figure 3.4b, upper), which include C1–C4 alkanes and alkenes. However, the turnover number (TON) of *MaNifH* (Figure 3.5c, lower), which is calculated based on the number of reduced carbons in products, is only 11% compared to that of *MaNifH* (Figure 3.5c, upper).
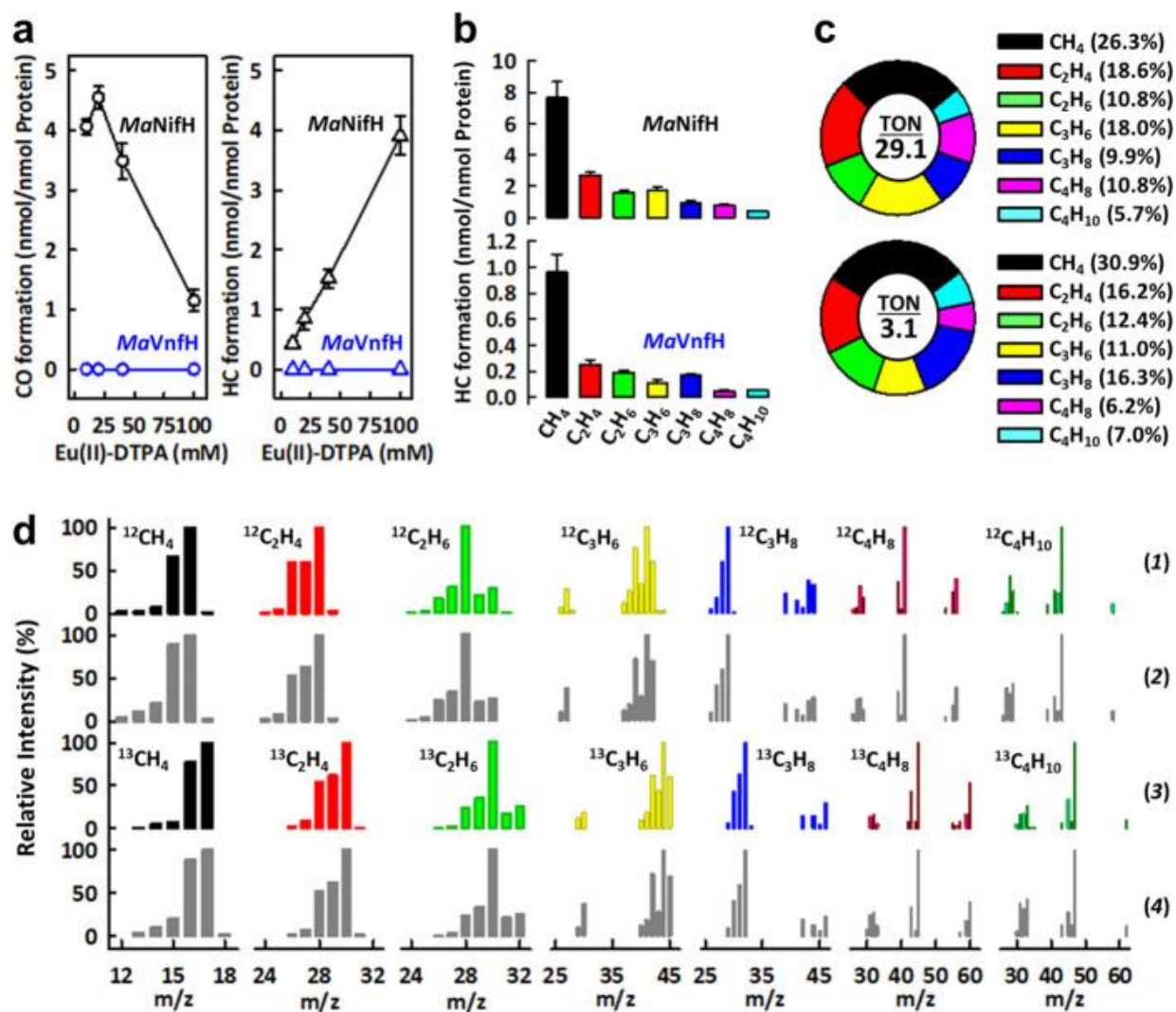
Figure 3.5 Reduction of CO_2 and CO by the all-ferrous *MaVnfH* and *MaNifH* proteins. (a) Yields of CO (left) and hydrocarbons (right) by *MaVnfH* (blue) and *MaNifH* (black) from CO_2 reduction at increasing Eu(II)-DTPA concentrations. Yields were calculated based on nmol of reduced C in CO or hydrocarbons per nmol protein. HC, hydrocarbons. (b) Identities and (c) distributions of hydrocarbons formed by *MaNifH* (upper) and *MaVnfH* (lower) from CO reduction at 100 mM Eu(II)-DTPA. TON, turnover number, was calculated based on the total nmol of reduced C in hydrocarbons generated per nmol of protein. (d) GC-MS analysis of the hydrocarbon products generated from the reduction of [12]CO (1) or [13]CO (3) by *MaVnfH*, shown in comparison with the fragmentation patterns of the corresponding ^{12}C-containing (2) or ^{13}C-labeled (4) hydrocarbon standards.

3.4 Conclusion

The observation of differential reactivities of the all-ferrous *MaVnfH* and *MaNifH* proteins is

important, as it highlights the crucial role of protein scaffolds in modulating the redox

properties and catalytic capabilities of the active-site [Fe$_4$S$_4$] centers of these proteins. More importantly, the fact that *MaVnfH* can adopt the all-ferrous state at a reduction potential that is achievable under physiological conditions [23, 70-72] suggests the possibility that more Fe proteins may achieve and utilize this state for various cellular functions at similar or perhaps even more positive reduction potentials. This finding bears significant relevance to the long-standing debate in the field as to whether the Fe protein can only shuttle between the [Fe$_4$S$_4$]$^{1+}$ and [Fe$_4$S$_4$]$^{2+}$ states to support a one-electron transfer during catalysis or if it can also shuttle between the [Fe$_4$S$_4$]^0 and [Fe$_4$S$_4$]$^{2+}$ state to enable a two-electron electron transfer under physiological conditions. [73-75] The latter scenario is particularly important for nitrogenase catalysis, as it would cut the ATP consumption for electron transfer by half and thereby improve the energy economy of nitrogen fixation by 2-fold in the cell. The observation reported herein provides a useful platform for further investigation into the redox properties of the Fe protein, which is crucial for expanding our understanding of the reaction mechanism of the nitrogenase enzyme and the cellular energetics of the nitrogen-fixing microorganisms.

CHAPTER 4

Investigation of the R101A Variant of *A. vinelandii* Iron Protein

4.1 Introduction

The structural basis and function of the iron protein has been discussed in chapter 1 and 2 in details. This chapter is mainly focused on the expression of *Azotobacter vinelandii* iron protein and R101A variant of *Azotobacter vinelandii* iron protein in *E. coli* and investigating its properties and potential.

4.2 Experimental Methods

Unless noted otherwise, chemicals and reagents were obtained from Fisher Scientific or Sigma-Aldrich. All protein work was performed under Ar gas at an O_2 concentration of less than 5 ppm.

4.2.1 Cell Growth and Protein Purification

Av*NifH-*Ec

Strain YM322EE contains his-tagged *Av*NifH on a pet-duet14b, *Isc*U with a T7 promoter, and untagged *Av*NifM on a pRSFDuet-1 in BL21 cells. The strain was made by transforming competent cells derived from the parent strain YM318EE, which contains his-tagged *Av*NifH on a pet-duet14b and untagged *Av*NifM on a pRSFDuet-1, with *Isc*U.

YM322EE was grown in 10L batches in a New Brunswick Scientific BioFlo415. The growth media consisted of lysogeny broth supplemented with 73mg/L $(NH_4)_2Fe(SO_4)_2(H_2O)_6$, 136mg/L L-Cys-HCl, 50mg/L kanamycin, 100mg/L ampicillin, and 34mg/L chloramphenicol. YM322EE was induced with IPTG at an O.D. of .8 and expressed at 21 ^{0}C for 14h. 20 L of culture yielded ~65g of cell paste. Following purification using Ni-IMAC, the protein was concentrated using Q-sepharose. ~150mg of dark brown protein was isolated.

Av*NifH-R101A-*Ec

Strain YM377EE contains his-tagged *Av*NifH R101A on a pet-duet14b, *Isc*U with a T7 promoter, and untagged *Av*NifM on a pRSFDuet-1 in BL21 cells. The strain was made by transforming competent cells derived from the parent strain YM371EE, which contains his-tagged *Av*NifH R101A on a pet-duet14b and untagged *Av*NifM on a pRSFDuet-1, with *Isc*U.

YM322EE was grown in 10L batches in a New Brunswick Scientific BioFlo415. The growth media consisted of lysogeny broth supplemented with 73mg/L $(NH_4)_2Fe(SO_4)_2(H_2O)_6$, 136mg/L L-Cys-HCl, 50mg/L kanamycin, 100mg/L ampicillin, and 34mg/L chloramphenicol. YM322EE was induced with IPTG at an O.D. of .8 and expressed at 21 ^{0}C for 14h. 20 L of culture yielded ~65g of cell paste. Following purification using Ni-IMAC, the protein was concentrated using Q-sepharose. ~150mg of dark brown protein was isolated.

4.2.2 SDS-PAGE Gel Analysis

SDS-PAGE analysis was performed using a 4-15% Mini-PROTEIN TGX precast gel (BioRad). The gel was run at 200 V and 50 mA for 40 min in TGX running buffer and stained with Coomassie Brilliant Blue.
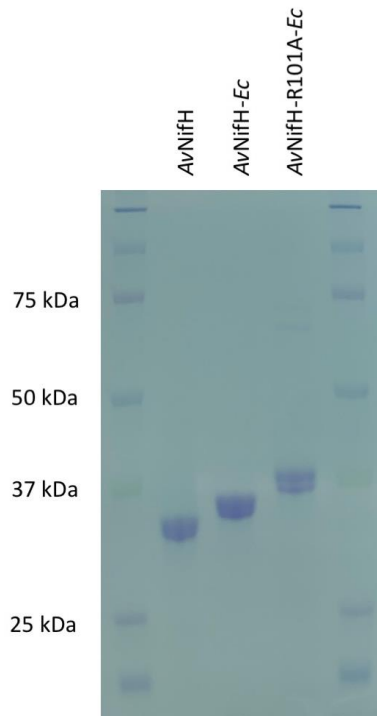
Figure 4.1 SDS-PAGE gel of isolated proteins.

4.2.3 Iron Determination

The iron (Fe) content of the proteins was determined by inductively coupled plasma optical emission spectroscopy (ICP-OES) using a Thermo Scientific iCAP7000 instrument. Each protein was mixed with 200 μL 1:1 volumetric ratio of concentrated sulfuric acid (H_2SO_4) and nitric acid (HNO_3) and heated at 250 °C for 30 minutes. This procedure was repeated until the solutions became clear/colorless. The room temperate solutions were diluted with 2% HNO_3 (vol/vol) to a total volume of 7.5 mL and analyzed on the Thermo Scientific iCAP7000 instrument. [42]

4.2.4 M-cluster Maturation Assay

The assay contained 25 mM Tris-HCl (pH 8), 20 mM $Na_2S_2O_4$, 0.8 mM MgATP, 1.6 mM $MgCl_2$, 0.5mM +/- homocitrate, 10 mM creatine phosphate, 8 units creatine kinase, 0.25 mM

49

molybdate (MoO_4^-), 1.4 mg AvNifH, 2 mg AvNifEN, 0.45 mg ΔAvNifB AvNifDK, and 1.0 mg iron protein (total volume of 1 mL). The mixture was incubated at 30 °C water bath for 30 minutes, followed by determination of enzymatic activities according to previously reported methods. [42]

4.2.5 Enzymatic Activity Assay

The assay contained 0.27 mg of AvNifDK, 0.15 mg of iron protein (AvNifH-Ec and AvNifH-R101A-Ec), 0.9 mM MgATP, 20 mM $Na_2S_2O_4$, 1.6 mM $MgCl_2$, 10 mM creatine phosphate, and 8 units creatine kinase (total volume of 1.0 mL). For C_2H_2 reduction assay, 0.1 atm C_2H_2, and 1 atm Ar were added to the headspace. [27, 35] Followed by 8 minutes incubation in 30 °C water bath. A total of 250 μL of headspace was injected onto a Grace 5664PC column on a gas chromatograph-flame ionization detector (GC-FID, SRI 8610) for each assay. High purity helium was used as a carrier gas at 20 PSI. Determination of C_2H_4 was performed using the previously reported method. [12, 48]

4.3 Results and Discussion

The metal analysis results of the two iron proteins indicate that these proteins have >80% [Fe_4S_4] cluster occupancy. However, the presence of iron in the form of [Fe_4S_4] with the ability to adopt three different oxidation states (0, +1, and +2) has to be determined by EPR spectroscopy.

Table 4.1 Metal analysis of the iron proteins

Protein	# Fe / dimer	% Occupancy
AvNifH-Ec	3.6 ± 0.4	90
AvNifH-R101A-Ec	3.2 ± 0.3	80

Specific activities for acetylene reduction determined that AvNifH-R101A-Ec variant to be inactive. In contrast AvNifH-Ec is about 97% active as the AvNifH from *Azotobacter vinelandii* (wild-type). Table 4.2 represents the specific and relative activities of iron proteins compared to the wild-type iron protein from *Azotobacter vinelandii* (AvNifH-wt).

Table 4.2 Cross-reactivities of the iron proteins with AvNifDK monitored by C_2H_2 substrate

Activities (nmol electron min^{-1} mg^{-1})		
Protein	Specific Activity	Relative Activity
AvNifH-wt	1534 ± 127	100
AvNifH-Ec	1486.5 ± 49	97
AvNifH-R101A-Ec	0	0

Table 4.3 The comparative effectiveness of the Fe proteins to synthesize the M-cluster, represented as a percent to AvNifH

Activities (nmol electron min^{-1} mg^{-1})		
Protein	Specific Activity	Relative Activity
AvNifH-wt	343.1 ± 18.9	100
AvNifH-Ec	334.1 ± 21.1	97.6
AvNifH-R101A-Ec	124.7 ± 11.5	36.4
Blank	139.5 ± 4.6	40.6

Table 4.4 The comparative effectiveness of the Fe proteins to synthesize the P-cluster, represented as a percent to *Av*NifH

Activities (nmol electron min^{-1} mg^{-1})		
Protein	**Specific Activity**	**Relative Activity**
***Av*NifH-wt**	361.8 ± 8.7	100
Av*NifH-*Ec	341.6 ± 18.0	94.4
Av*NifH-R101A-*Ec	17.5 ± 1.3	4.8
Blank	22.6 ± 3.2	6.24

Tables 4.3 and 4.4 provide the comparative effectiveness of the Fe proteins to synthesize the M- and P-cluster, respectively. The specific and relative activities of iron proteins are relative to the wild-type iron protein from *Azotobacter vinelandii*. In both M- and P-cluster maturation, *Av*NifH-*Ec* is proven as active as the wild-type *Av*NifH-wt, while the *Av*NifH-R101A-*Ec* shows no activity in regard to the acetylene reduction, M- and P-cluster maturation.

Based on these results *Av*NifH-*Ec* is a suitable candidate for co-expression with *Av*NifDK in *E. coli* to get a fully functioning nitrogenase system in *E. coli* as the future goal of this project.

References

1. Ashby, G. A., Dilworth, M. J., & Thorneley, R. N. F. Klebsiella pneumoniae nitrogenase. Inhibition of hydrogen evolution by ethylene and the reduction of ethylene to ethane. *Biochemical Journal*, **1987**, 247(3), 547–554.

2. Beecher, G. R., & Whitten, B. K. Ammonia determination: Reagent modification and interfering compounds. *Analytical Biochemistry*, **1970**, 36(1), 243–246.

3. Bertsova, Y. V., Bogachev, A. V., & Skulachev, V. P. Noncoupled NADH: Ubiquinone oxidoreductase of Azotobacter vinelandii is required for diazotrophic growth at high oxygen concentrations. *Journal of Bacteriology*, **2001**, 183(23), 6869–6874.

4. Brigle, K. E., Setterquist, R. A., Dean, D. R., Cantwell, J. S., Weiss, M. C., & Newton, W. E. Site-directed mutagenesis of the nitrogenase MoFe protein of Azotobacter vinelandii. *Proceedings of the National Academy of Sciences of the United States of America*, **1987**, 84(20), 7066–7069.

5. Brill, W. J. Biochemical genetics of nitrogen fixation. *Microbiological Reviews*, **1980**, 44(3), 449–467.

6. Bulen, W. A., & LeComte, J. R. The nitrogenase system from Azotobacter: Two-enzyme requirement for nitrogen reduction, ATP-dependent hydrogen evolution, and ATP hydrolysis. *Proceedings of the National Academy of Sciences of the United States of America*, **1966**, 56(3), 979–986.

7. Burgess, B. K. The iron-molybdenum cofactor of nitrogenase. *Chemical Reviews*, **1990**, 90(8), 1377–1406.

8. Burgess, B. K., Jacobs, D. B., & Stiefel, E. I. Large-scale purification of high activity Azotobacter vinelandii nitrogenase. *Biochimica et Biophysica Acta—Enzymology*, **1980**,614(1), 196–209.

9. James B. Howard and Douglas C. Rees, Structural Basis of Biological Nitrogen Fixation, *Chemical Reviews*, **1996**, 96 (7), 2965-2982.

10. Hoffman, B. M.; Lukoyanov, D.; Yang, Z.-Y. Y.; Dean, D. R.; Seefeldt, L. C. Mechanism of Nitrogen Fixation by Nitrogenase: *The Next Stage. Chem. Rev.*, **2014**, 114, 4041–4062.

11. Stefan Burén, Emilio Jiménez-Vicente, Carlos Echavarri-Erasun, and Luis M. Rubio Biosynthesis of Nitrogenase Cofactors, *Chemical Reviews*, **2020**, 120 (12), 4921-4968.

12. Ribbe M. W., Hu Y., Hodgson K. O., Hedman B. Biosynthesis of nitrogenase metalloclusters. *Chem Rev.*, **2014**,114(8):4063-4080.

13. Hausinger, R. P.; Howard, Thiol reactivity of the nitrogenase Fe-protein from Azotobacter vinelandii, *J. B. J. Biol. Chem.*, **1983**, 258, 13486.

14. Strop, P.; Takahara, P.M.; Chiu, H.-J.; Angove, H.C.; Burgess, B.K.; Rees, D.C. Crystal structure of the all-ferrous $[4Fe-4S]^0$ form of the nitrogenase iron protein from Azotobacter vinelandii. *Biochemistry*, **2001**, 40, 651–656.

15. Jasniewski, A.J.; Sickerman, N.S.; Hu, Y.; Ribbe, M.W. The Fe Protein: An Unsung Hero of Nitrogenase. *Inorganics*, **2018**, 6, 25.

16. Burgess, B. K. & Lowe, D. J. Mechanism of molybdenum nitrogenase. *Chem. Rev.*, **1996**, 96, 2983–3011.

17. Rees, D. C. Dinitrogen reduction by nitrogenase: if N_2 isn't broken, it can't be fixed. *Curr. Opin. Struc. Biol.*, **1993**, 3, 921–928.

18. Walker, G. A. & Mortenson, L. E. Effect of magnesium adenosine 5'-triphosphate on the accessibility of the iron of clostridial azoferredoxin, a component of nitrogenase. *Biochemistry*, **1974**, 13, 2382–2388.

19. Ljones, T. & Burris, R. H. Nitrogenase: the reaction between iron protein and bathophenanthrolinedisulfonate as a probe for interactions with MgATP. *Biochemistry*, **1978**, 17, 1866–1872.

20. Deits, T. L. & Howard, J. B. Kinetics of MgATP-dependent iron chelation from the Fe-protein of the Azotobacter vinelandii nitrogenase complex. Evidence for two states. J. *Biol. Chem.*, **1989**, 264, 6619–6628.

21. Chen, L. et al. MgATP-induced conformational changes in the iron protein from Azotobacter vinelandii, as studied by small-angle x-ray scattering. *J. Biol. Chem.*, **1994**, 269, 3290–3294.

22. Tezcan, F. A., Kaiser, J. T., Howard, J. B. & Rees, D. C. Structural evidence for asymmetrical nucleotide interactions in nitrogenase. *J. Am. Chem. Soc.*, **2015**, 137, 146–149.

23. Schindelin, H., Kisker, C., Schlessman, J. L., Howard, J. B. & Rees, D. C. Structure of ADP·AlF$_4^-$ stabilized nitrogenase complex and its implications for signal transduction. *Nature*, **1997**, 387, 370–376.

24. Kim, J. & Rees, D. C. Crystallographic structure and functional implications of the nitrogenase molybdenum-iron protein from Azotobacter vinelandii. *Nature*, **1992**, 360, 553–560.

25. Van Stappen, C., Decamps, L. & DeBeer, S. Preparation and spectroscopic characterization of lyophilized Mo nitrogenase. *J. Biol. Inorg. Chem.*, **2021**, 26, 81–91.

26. Wenke, B. B., Spatzal, T., & Rees, D. C., State Assignments of the Iron Atoms in the [4Fe:4S]$^{2+/1+/0}$ States of the Nitrogenase Fe-Protein. *Angewandte Chemie*, **2019**, 58(12), 3894–3897.

27. Hu, Y.; Ribbe, M. W. Nitrogenases—A Tale of Carbon Atom. *Angew. Chem.*, **2016**, 128, 8356.

28. Lee, C.C.; Hu, Y.; Ribbe, M. W. Vanadium Nitrogenase Reduces CO. *Science*, **2010**, 329, 642.

29. Hu, Y.; Lee, C. C.; Ribbe, M. W. Vanadium Nitrogenase: A two-hit wonder? *Dalton Trans.*, **2012**, 41, 1118.

30. Hu, Y.; Lee, C. C.; Ribbe, M. W. Extending the Carbon Chain: Hydrocarbon Formation Catalyzed by Vanadium/molybdenum Nitrogenases. *Science*, **2011**, 333, 753.

31. Yang, Z. Y.; Dean, D. R.; Seefeldt, L. C. Molybdenum Nitrogenase Catalyzes the Reduction and Coupling of CO to form Hydrocarbons. *J. Biol. Chem.*, **2011**, 286, 19417.

32. Seefeldt L. C., Hoffman B. M., Dean D. R. Mechanism of Mo-dependent nitrogenase. *Annu. Rev. Biochem.*, **2009**;78:701-722.

33. Spatzal, T.; Aksoyoglu, M.; Zhang, L.; Andrade, S. L.; Schleicher, E.; Weber, S.; Rees, D. C.; Einsle, O. Evidence for Interstitial Carbon in Nitrogenase FeMo Cofactor. *Science,* **2011**, 334 (6058), 940–940.

34. Hoover, T. R.; Imperial, J.; Ludden, P. W.; Shah, V. K. Homocitrate Is a Component of the Iron-Molybdenum Cofactor of Nitrogenase. *Biochemistry,* **1989**, 28 (7), 2768–2771.

35. Hu, Y.; Ribbe, M. W. Nitrogenase and Homologs. *J. Biol. Inorg. Chem.*, **2015**, 20, 435.

36. Available at the open Joint Genome Institute (JGI) database (https://img.jgi.doe.gov/cgi-bin/m/main.cgi).

37. Schmid, B.; Einsle, O.; Chiu, H. J.; Willing, A.; Yoshida, M.; Howard, J. B.; Rees, D. C. Biochemical and Structural Characterization of the Cross-linked Complex of Nitrogenase: Comparison to the ADP-AlF$_4^{(-)}$-stabilized Structure. *Biochemistry,* **2002**, 41, 15557.

38. Kim, J.; Rees, D. C. Structural Models for the Metal Centers in the Nitrogenase Molybdenum-Iron Protein. *Science,* **1992**, 257 (5077), 1677–1682.

39. Tyree, B.; Webster, D. A. Electron-accepting Properties of Cytochrome o Purified from Vitreoscilla. *J. Biol. Chem.*, **1978**, 253, 7635.

40. Rebelein, J. G.; Stiebritz, M. T.; C. C. Lee, C. C.; Hu, Y. Activation and Reduction of Carbon Dioxide by Nitrogenase Iron Proteins. *Nat. Chem. Biol.*, **2017**, 13, 147-149.

41. Vincent, K. A.; Tilley, G. J.; Quammie, N. C.; Streeter I.; Burgess, B. K.; Cheesman, M. R.; Armstrong, F. A. Instantaneous, Stoichiometric Generation of Powerfully Reducing States of Protein Active Sites Using Eu(II) and Polyaminocarboxylate Ligands. *Chem. Commun. (Camb),* **2003**, 2590.

42. Hiller, C. J.; Stiebritz, M. T.; Lee, C. C.; Liedtke, J.; Hu, Y. Tuning Electron Flux through Nitrogenase with Methanogen Iron Protein Homologues. *Chem. Eur. J.,* **2017**, 23, 16152-16156

43. Arnold K.; L. Bordoli, J. Kopp, T. Schwede. The SWISS-MODEL workspace: A Web-based Environment for Protein Structure Homology Modelling. *Bioinformatics,* **2006**, 22, 195.

44. Comeau, S. R.; Gatchell, D. W.; Vajda, S.; Camacho, C. J. ClusPro: A Fully Automated Algorithm for Protein-protein Docking. *Nucleic Acids Res.*, **2004**, 32, W96.

45. Hu, Y.; Fay, A. W.; Dos Santos, P. C.; Naderi, F.; Ribbe, M. W. Characterization of Azotobacter vinelandii nifZ Deletion Strains: Indication of Stepwise MoFe Protein Assembly. *J. Biol. Chem.*, **2004**, 279 (52), 54963–54971.

46. Burgess, B. K.; Jacobs, D. B.; Stiefel, E. I. Large-Scale Purification of High Activity Azotobacter vinelandii Nitrogenase. Biochim. Biophys. *Acta, Enzymol.,* **1980**, 614 (1), 196–209.

47. Ribbe, M. W. Nitrogen Fixation: Methods and Protocols, *Humana,* **2011**.

48. Angove, H. C.; Yoo, S. J.; Menck, E.; Burgess, B. K. An All-ferrous State of the Fe Protein of Nitrogenase, Interaction with Nucleotides and Electron Transfer to the MoFe Protein. *J. Biol. Chem.*, **1998**, 273, 26330.

49. Schilter, D.; Camara, J. M.; Huynh, M. T.; Hammes-Schiffer, S.; Rauchfuss, T. B. Hydrogenase enzymes and their synthetic models: the role of metal hydrides. *Chem. Rev.*, **2016**, 116, 8693–8749.

50. Mühlenhoff, U.; Hoffmann, B.; Richter, N.; Rietzschel, N.; Spantgar, F.; Stehling, O.; Uzarska, M. A.; Lill, R. Compartmentalization of iron between mitochondria and the cytosol and its regulation. *Eur. J. Cell Biol.*, **2015**, 94, 292–308.

51. O'Brien, E.; Holt, M. E.; Thompson, M. K.; Salay, L. E.; Ehlinger, A. C.; Chazin, W. J.; Barton, J. K. The [4Fe4S] cluster of human DNA primase functions as a redox switch using DNA charge transport. *Science,* **2017**, 355, 1789.

52. Mettert, E. L.; Kiley, P. J. Fe-S proteins that regulate gene expression. *Biochim. Biophys. Acta, Mol. Cell Res.*, **2015**, 1853, 1284–1293.

53. Rutledge, H. L.; Tezcan, F. A. Electron transfer in nitrogenase. *Chem. Rev.,* **2020**, 120, 5158–5193.

54. Jasniewski, A. J.; Lee, C. C.; Ribbe, M. W.; Hu, Y. Reactivity, mechanism, and assembly of the alternative nitrogenases. *Chem. Rev.,* **2020**, 120, 5107–5157.

55. Buscagan, T. M.; Rees, D. C. Rethinking the nitrogenase mechanism: activating the active site. *Joule*, **2019**, 3, 2662–2678.

56. Lee, C. C.; Stiebritz, M. T.; Hu, Y. Reactivity of [Fe$_4$S$_4$] clusters toward C1 substrates: mechanism, implications, and potential applications. *Acc. Chem. Res.,* **2019**, 52, 1168–1176.

57. Sippel D & Einsle O. The structure of vanadium nitrogenase reveals an unusual bridging ligand. *Nat. Chem. Biol.,* **2017**, 13, 956-960.

58. Rohde M, Trncik C, Sippel D, Gerhardt S & Einsle O. Crystal structure of VnfH, the iron protein component of vanadium nitrogenase. *J. Biol. Inorg. Chem.*, **2018**, 23, 1049-1056.

59. Rettberg LA, Kang W, Stiebritz MT, Hiller CJ, Lee CC, Liedtke J, Ribbe MW & Hu Y. Structural analysis of a nitrogenase iron protein from *Methanosarcina acetivorans*:

Implications for CO_2 capture by a surface-exposed [Fe_4S_4] cluster. *mBio,* **2019**, 10, e01497-19

60. Stiebritz, M. T.; Hiller, C. J.; Sickerman, N. S.; Lee, C. C.; Tanifuji, K.; Ohki, Y.; Hu, Y. Ambient conversion of CO_2 to hydrocarbons by biogenic and synthetic [Fe_4S_4] clusters. *Nat. Catal.*, **2018**, 1, 444–451.

61. Rofer-DePoorter, C. K. A comprehensive mechanism for the Fischer–Tropsch synthesis. *Chem. Rev.,* **1981**, 81, 447–474.

62. Leggate, E. J.; Bill, E.; Essigke, T.; Ullmann, G. M.; Hirst, J. Formation and characterization of an all-ferrous Rieske cluster and stabilization of the $[2Fe-2S]^0$ core by protonation. *Proc. Natl. Acad. Sci. U. S. A.,* **2004**, 101, 10913–10918.

63. Vincent, K. A.; Tilley, G. J.; Quammie, N. C.; Streeter, I.; Burgess, B. K.; Cheesman, M. R.; Armstrong, F. A. Instantaneous, stoichiometric generation of powerfully reducing states of protein active sites using Eu(II) and polyaminocarboxylate ligands. *Chem. Commun.* (Cambridge, U. K.) **2003**, 20, 2590–2591.

64. Ribbe, M. W.; Hu, Y.; Guo, M.; Schmid, B.; Burgess, B. K. The FeMoco-deficient MoFe protein produced by a nifH deletion strain of Azotobacter vinelandii shows unusual P-cluster features. *J. Biol. Chem.,* **2002**, 277, 23469-23476.

65. Sawyer, D. T.; Sobkowiak, A.; Roberts, J. L. Electrochemistry for Chemists, 2nd Edition. Wiley, New York, NY, **1995**

66. Mayhew, S. G. The redox potential of dithionite and SO_2^- from equilibrium reactions with flavodoxins, methyl viologen and hydrogen plus hydrogenase. *Eur. J. Biochem.,* **1978**, 85, 535–547.

67. Yoshizawa, J. M.; Blank, M. A.; Fay, A. W.; Lee, C. C.; Wiig, J. A.; Hu, Y.; Hodgson, K. O.; Hedman, B.; Ribbe, M. W. Optimization of FeMoco maturation on NifEN. *J. Am. Chem. Soc.,* **2009**, 131, 9321–9325.

68. Yoo, S. J.; Angove, H. C.; Burgess, B. K.; Hendrich, M. P.; Münck, E. Mössbauer and integer-spin EPR studies and spin-coupling analysis of the $[4Fe-4S]^0$ cluster of the Fe protein from *Azotobacter vinelandii* nitrogenase. *J. Am. Chem. Soc.,* **1999**, 121, 2534–2545.

69. Guo, M.; Sulc, F.; Ribbe, M. W.; Farmer, P. J.; Burgess, B. K. Direct assessment of the reduction potential of the $[4Fe-4S]^{(1+/0)}$ couple of the Fe protein from *Azotobacter vinelandii. J. Am. Chem. Soc.*, **2002**, 124, 12100–12101.

70. Hosseinzadeh, P.; Lu, Y. Design and fine-tuning redox potentials of metalloproteins involved in electron transfer in bioenergetics. *Biochim. Biophys. Acta, Bioenerg.,* **2016**, 1857, 557–581

71. Liu, J.; Chakraborty, S.; Hosseinzadeh, P.; Yu, Y.; Tian, S.; Petrik, I.; Bhagi, A.; Lu, Y. Metalloproteins containing cytochrome, iron-sulfur, or copper redox centers. *Chem. Rev.*, **2014**, 114, 4366–4469.

72. Gao-Sheridan, H. S.; Pershad, H. R.; Armstrong, F. A.; Burgess, B. K. Discovery of a novel ferredoxin from *Azotobacter vinelandii* containing two [4Fe-4S] clusters with widely differing and very negative reduction potentials. *J. Biol. Chem.,* **1998**, 273, 5514–5519.

73. Howard, J. B.; Rees, D. C. How many metals does it take to fix N_2? A mechanistic overview of biological nitrogen fixation. *Proc. Natl. Acad. Sci. U. S. A.,* **2006**, 103, 17088–17093.

74. Erickson, J. A.; Nyborg, A. C.; Johnson, J. L.; Truscott, S. M.; Gunn, A.; Nordmeyer, F. R.; Watt, G. D. Enhanced efficiency of ATP hydrolysis during nitrogenase catalysis utilizing reductants that form the all-ferrous redox state of the Fe protein. *Biochemistry,* **1999**, 38, 14279–14285.

75. Lowery, T. J.; Wilson, P. E.; Zhang, B.; Bunker, J.; Harrison, R. G.; Nyborg, A. C.; Thiriot, D.; Watt, G. D. Flavodoxin hydroquinone reduces Azotobacter vinelandii Fe protein to the all-ferrous redox state with a S = 0 spin state. *Proc. Natl. Acad. Sci. U. S. A.,* **2006**, 103, 17131–17136.